



# Voltammetric analysis of epinephrine using glassy carbon electrode modified with nanocomposite prepared from Co-Nd bimetallic nanoparticles, alumina nanoparticles and functionalized multiwalled carbon nanotubes

Shreanshi Agrahari<sup>1</sup> · Ankit Kumar Singh<sup>1</sup> · Ravindra Kumar Gautam<sup>1</sup> · Ida Tiwari<sup>1</sup>

Received: 29 July 2022 / Accepted: 12 October 2022 / Published online: 25 October 2022  
© The Author(s), under exclusive licence to Springer-Verlag GmbH Germany, part of Springer Nature 2022

## Abstract

Herein, we investigated the electrochemical behaviour of fMWCNTs decorated with Co-Nd bimetallic nanoparticles and alumina nanoparticles (Co-Nd/Al<sub>2</sub>O<sub>3</sub>@fMWCNTs). The nanocomposites were synthesised using simple mechanical mixing and characterised by FT-IR, XRD, UV–visible studies, SEM, TEM and EDAX. Moreover, the crystalline size of the synthesised nanoparticles was also calculated using XRD data (Debye–Scherer formula) and was found in the nm range. The electrochemical behaviour of epinephrine (EP) was examined in the presence of Co-Nd/Al<sub>2</sub>O<sub>3</sub>@fMWCNTs nanocomposite modified glassy carbon electrode (GCE) using various electrochemical techniques such as cyclic voltammetry (CV), differential pulse voltammetry (DPV), electrochemical impedance spectroscopy (EIS), and chronocoulometry. Among all the above-mentioned techniques, the DPV response of the modified Co-Nd/Al<sub>2</sub>O<sub>3</sub>@fMWCNTs/GCE under optimal circumstances revealed a dual linear range (0.2 to 4000 μM and 4000 to 14,000 μM) and LOD of 0.015 μM (*S/N* = 3). The sensitivities were determined to be 0.00323 μAμM<sup>-1</sup> and 0.0004 μAμM<sup>-1</sup> in 0.2 to 4000 μM and 4000 to 14,000 μM concentration ranges. Using chronocoulometry, the surface coverage of Co-Nd/Al<sub>2</sub>O<sub>3</sub>@fMWCNTs/GCE was calculated to be 1.37 × 10<sup>-8</sup> mol cm<sup>-2</sup>. The fabricated Co-Nd/Al<sub>2</sub>O<sub>3</sub>@fMWCNTs/GCE demonstrated remarkable repeatability, with an RSD of 0.09%, and storage stability of 3 weeks, with 89.6% current retention. Lastly, it was found that Co-Nd/Al<sub>2</sub>O<sub>3</sub>@fMWCNTs/GCE worked well for EP analysis in a variety of biological fluids.

**Keywords** Chronocoulometry · Bimetallic nanoparticles · Functionalized MWCNTs · Epinephrine · Modified GCE · Electrochemical sensor

Responsible Editor: George Z. Kyzas

## Highlights

- Co/Nd bimetallic nanoparticles and alumina nanoparticles decorated over fMWCNTs (Co-Nd/Al<sub>2</sub>O<sub>3</sub>@fMWCNTs) were prepared through simple mechanical mixing.
- Several electrochemical techniques like CV, DPV, EIS, and chronocoulometry were employed for EP sensing.
- Concentration ranges from 0.2 to 14,000 μM, with a detection limit of 0.015 μM (*S/N* = 3).
- Surface coverage ( $\Gamma_s$ ) was calculated to be 1.37 × 10<sup>-8</sup> mol cm<sup>-2</sup> at Co-Nd/Al<sub>2</sub>O<sub>3</sub>@fMWCNTs/GCE.
- The developed sensor shows good selectivity, reproducibility, and stability.
- The modified GCE was effectively used for the analysis of EP in blood serum and urine samples.

Extended author information available on the last page of the article

## Introduction

Epinephrine (EP), also known as adrenaline, acts both as a hormone and a neurotransmitter that has a significant biological and pharmacological role in the mammalian central nervous system (Cannon et al. 1929). EP is capable of controlling various processes that include heartbeat and blood pressure acceleration (Struthers et al. 2016), easing acute respiratory distress syndrome (Fernando et al. 2021) and it is also useful in treating several illnesses like asthma, bronchitis, cardiac arrest, anaphylaxis, and hypertension (Agboola et al. 2009). Since EP is a stress releasing hormone, its injections were given during COVID-19 pandemic to reduce the cardiac impact (Mahnaz and Ansarian 2020). Moreover, fluctuations in the EP concentrations lead to numerous

diseases, such as Parkinson's disease (Spencer et al. 1998), multiple sclerosis (Liou et al. 2006) and Alzheimer's disease (Burke et al. 1988). The quantity of EP in human fluid is one of the most essential screening tools for monitoring its therapeutic treatment and for determining the potential mediator in affected individuals (Raymondos et al. 2000). Hence, there is a requirement to develop an efficient technique for EP detection in different biological fluids (Oruch et al. 2014). Several conventional methods have been used for EP determination and were based on high performance liquid chromatography (Sabbioni et al. 2004), fluorimetry (Cañizares and de Castro 1995), capillary electrophoresis (Lin et al. 2004), chemiluminescence (Michałowski and Hałaburda 2001) and electrochemical analysis (Garrido et al. 1997; Ni et al. 1999).

The conventional techniques offer various advantages that include high sensitivity and significant reliability. However, they suffer from some limitations that include poor selectivity, tedious and time-consuming measurements, requirements for pre-treatment for sample extraction, and costly instrumentation (Belluzo et al. 2008). Although, electrochemical sensors are simple, cost-effective, portable and small-sized, they also provide high selectivity and sensitivity for EP sensing (Georgakilas et al. 2007) (Tezerjani et al. 2017). However, electrochemical approaches have certain drawbacks in the EP detection. An irreversible redox reaction occurs at a bare electrode, resulting in a large over potential due to the slow electrode kinetics at the electrode's surface (Garrido et al. 1997). Moreover, since uric acid and ascorbic acid act as interfering analytes in EP sensing, its electrochemical analysis becomes difficult (Manjunatha et al. 2018). Hence, to overcome the above mentioned challenges, electrode must be modified with a suitable nanocomposite material (Sanghavi et al. 2015).

Nanomaterials are being dominated by their nanoscale design, which provides several attractive properties, such as enhanced surface to volume ratio, which helps in fast reaction kinetics measurements with greater sensing performance for EP determination (Ramgir et al. 2010) (Iost et al. 2011). Multiwalled carbon nanotubes (MWCNTs) have gained substantial significance among researchers owing to their attractive properties such as enormous surface area which acts as a supporting material with photocatalytic features, large thermal and chemical stability and better electrical conductivity (Yang et al. 2015). However, pristine MWCNTs may not be used in the modification of electrodes due to a lack of solubility in water (Pérez-López and Merkoçi 2012). Hence, functionalization of MWCNTs can be performed to improve their dispersion in water, which is useful in enhancing the electrode performance for EP sensing (Hu et al. 2010).

Alumina nanoparticles have got several applications due to attractive features such as catalysing electrochemical

reactions and providing a large surface to volume ratio, which are useful in electrode fabrication (Kusuma et al. 2020). Bimetallic nanoparticles have been broadly used in electrochemical sensing due to their unique features such as outstanding electro catalytic activity and quicker response rate (Zhang et al. 2018). However, these nanoparticles show several limitations of easy aggregation, which act as an obstacle in electrode fabrication. Therefore, a suitable support is a prerequisite needed to prevent metal nanoparticles from aggregation (Eksin et al. 2015). Hence, the nanocomposite was synthesised using Co-Nd bimetallic nanoparticles, alumina nanoparticles and fMWCNTs (Co-Nd/Al<sub>2</sub>O<sub>3</sub>@fMWCNTs). Furthermore, enhanced electro catalytic properties and increased sensitivity that were realised might be due to the synergistic effects of the synthesised Co-Nd bimetallic and alumina nanoparticles attached to fMWCNTs.

The present work aimed to create a low-cost, simple-to-make and fast response EP sensor based on Co-Nd/Al<sub>2</sub>O<sub>3</sub>@fMWCNTs nanocomposite modified GCE with a wide concentration range. This is the first time that Co-Nd bimetallic NPs and alumina NPs supported on fMWCNT-based nanocomposite were synthesised and immobilised on GCE for EP sensing. This paper proposes a straightforward electrode modification approach. Surface coverage ( $\Gamma_s$ ) was calculated at Co-Nd/Al<sub>2</sub>O<sub>3</sub>-fMWCNTs/GCE using chronocoulometry. Furthermore, interference studies were also performed in the presence of various analytes such as Na<sup>+</sup>, Cl<sup>-</sup>, K<sup>+</sup>, NO<sub>3</sub><sup>-</sup>, para-amino phenol, glucose, estradiol, dopamine, uric acid and ascorbic acid. The fabricated Co-Nd/Al<sub>2</sub>O<sub>3</sub>@fMWCNTs/GCE was also tested for repeatability, reproducibility and stability. The modified Co-Nd/Al<sub>2</sub>O<sub>3</sub>@fMWCNTs/GCE is a simple, sensitive and efficient electrochemical sensor for EP detection both in blood serum and urine samples.

## Experimental section

### Chemicals and reagents

All the chemicals used in the experiment were of analytical grade. Epinephrine and multiwalled carbon nanotubes (> 90% purity, OD 110–170 nm, length 5–9 μm, purity) were bought from Sigma Aldrich. Alfa-Aesar, Loba Chemie and Merck provided cobalt nitrate hexahydrate (Co(NO<sub>3</sub>)<sub>2</sub>·6H<sub>2</sub>O), neodymium oxide (Nd<sub>2</sub>O<sub>3</sub>) and aluminium nitrate nonahydrate (Al(NO<sub>3</sub>)<sub>3</sub>·9H<sub>2</sub>O, respectively). Ethylene glycol (CH<sub>2</sub>OH)<sub>2</sub>, sodium hydroxide (NaOH) and citric acid were procured from Himedia Laboratories Pvt. Ltd, and s-d fine chem. Ltd, respectively. Using a suitable amount of ethanol (C<sub>2</sub>H<sub>5</sub>OH), 0.1 M stock solution of EP was prepared. Aqueous solutions of 0.1 M sodium dihydrogen phosphate (NaH<sub>2</sub>PO<sub>4</sub>) and disodium hydrogen phosphate (Na<sub>2</sub>HPO<sub>4</sub>) were made individually and mixed in an

approximate ratio to get a 0.1 M phosphate buffer solution (PBS, pH 7.0). All solutions were made using triple distilled water.

## Instrumentations

To examine the morphology of the synthesised nanomaterials, scanning electron microscopy (SEM; coupled with energy dispersive X-ray analysis; EDAX) was performed using Zeiss EVO 18 Research. Furthermore, to study the morphology of the Co-Nd/Al<sub>2</sub>O<sub>3</sub>@fMWCNTs nanocomposite, transmission electron microscope (TEM) was carried out using TECHNAI G<sup>2</sup> 20 TWIN, FE, USA. The X-ray diffraction (XRD) pattern of the produced nanocomposite material was examined using Cu K $\alpha$  radiation on a D8 Advance/Discover Bruker Germany Diffractometer for characterisation of structure with a 2 $\theta$  range from 5 to 72°. The Fourier transform infrared spectra (FT-IR) of developed nanomaterials diluted in KBr pellets were examined on a Perkin Elmer (Spectrum Two) Fourier transform infrared spectrophotometer. The UV–visible studies were done using a UV–visible spectrometer Hitachi U-3900, Japan. All electrochemical measurements were analysed on an Autolab electrochemical workstation (TYPE III) having NOVA 1.8.17 software. The conventional three-electrode system employing bare and modified GCE as the working electrode, saturated Ag/AgCl as the reference electrode, and platinum wire as a counter electrode is used in the electrochemical system.

## Methods

### Synthesis of Co-Nd bimetallic nanoparticles

For the preparation of Co-Nd bimetallic nanoparticles, aqueous solutions of cobalt nitrate hexahydrate (Co(NO<sub>3</sub>)<sub>2</sub>·6H<sub>2</sub>O) (25 mM, 10 mL) and neodymium oxide (Nd<sub>2</sub>O<sub>3</sub>) (25 mM, 10 mL) were prepared separately. Both the solutions were mixed together, and ethylene glycol (CH<sub>2</sub>OH)<sub>2</sub> (10 mM, 5 mL) was added dropwise and then heated for 10 min at 95 °C. Furthermore, to maintain pH 9.0, NaOH was added. Then, the mixture was kept for an hour at 95 °C with constant stirring. Finally, the precipitate was cleaned with triple distilled water and ethanol and then dried at 80 °C.

### Synthesis of alumina nanoparticles

Alumina nanoparticles were synthesised using the auto-combustion method as reported earlier (Raghavendra et al. 2014). Typically, an aqueous solution of aluminium nitrate nonahydrate (Al(NO<sub>3</sub>)<sub>3</sub>·9H<sub>2</sub>O) (0.5 M, 100 mL) was prepared, followed by a slow addition of an aqueous solution of citric acid (1 M, 25 mL). The resultant mixture was kept at 70 °C by magnetic stirring. After sometimes, when the

solution becomes grey, the magnetic stirrer is removed. Furthermore, heating was continued until water was completely removed from the solution and a yellow powder was obtained. The resultant powder was calcined at 1000 °C to get pure white alumina powder.

### Synthesis Co-Nd/Al<sub>2</sub>O<sub>3</sub>@fMWCNTs nanocomposite

Before the synthesis of nanocomposites, MWCNTs were functionalized. For this, a dispersed solution of MWCNTs (40 mg, 40 mL) were made using concentrated nitric acid. The resulting mixture was ultrasonically agitated for 1 h under reflux conditions at 120 °C for 4 h. The black precipitates were collected and washed with triple distilled water and ethanol. Also, it was dried at 80 °C (Datsyuk et al. 2008). The Co-Nd/Al<sub>2</sub>O<sub>3</sub>@fMWCNTs nanocomposite was synthesised as represented in Fig. 1. For this, an equivalent amount of Co-Nd bimetallic nanoparticles, Al<sub>2</sub>O<sub>3</sub> nanoparticles and f-MWCNTs was taken and then ethanolic dispersion (25 mg in 10 mL) of Co-Nd bimetallic NPs, Al<sub>2</sub>O<sub>3</sub> and f-MWCNTs was prepared separately by dissolving them in ethanol and ultrasonicated for 4 h. Furthermore, all of them were mixed together and further sonicated for an hour. The reaction mixture was refluxed at 80 °C for 48 h. The produced precipitate was filtered, washed many times with triple distilled water and ethanol, which helps in removing any unreacted impurities. Furthermore, it was dried in a vacuum oven at 80 °C to get a completely dried product.

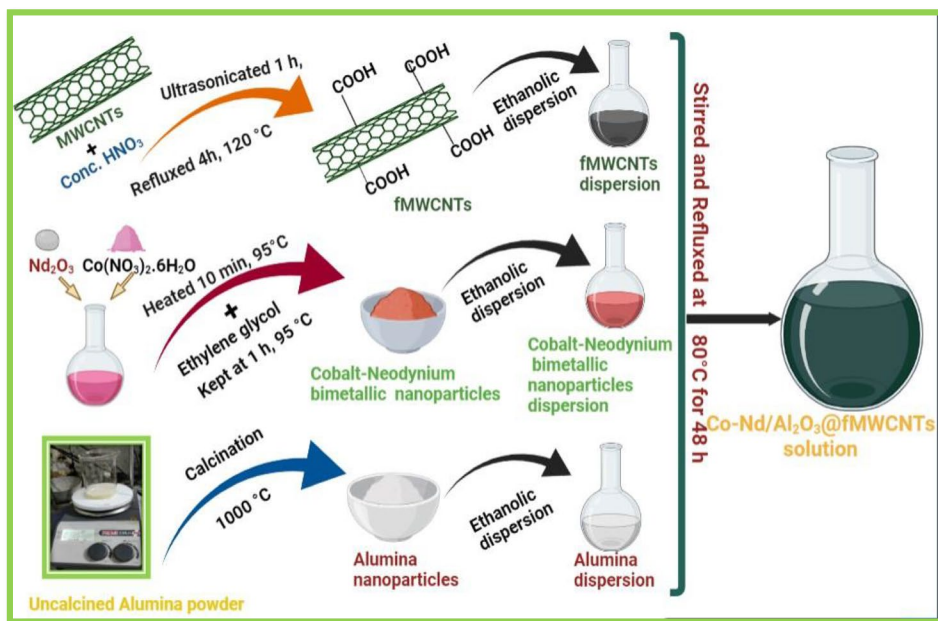
### Fabrication of Co-Nd/Al<sub>2</sub>O<sub>3</sub>@fMWCNTs nanocomposite modified GCE

Prior to modification, GCE was thoroughly polished with alumina powder of different sizes (1.0  $\mu$ m, 0.3  $\mu$ m, 0.05  $\mu$ m) successively to get a shining mirror-like surface. It was also ultrasonically treated for 30 s each with triple distilled water and acetone. The polished GCE was modified using Co-Nd/Al<sub>2</sub>O<sub>3</sub>@fMWCNTs nanocomposite material. For this, 2 mg of the synthesised composite material was dispersed through ultra-sonication in 1 mL of DMF for 2 h. After that, drop casting was done on bare GCE using 20  $\mu$ L of the prepared dispersed solution and kept at room temperature for overnight drying. The fabricated electrode was used as a working electrode for different electrochemical measurements. In a similar manner, Co-Nd/GCE, Al<sub>2</sub>O<sub>3</sub>/GCE, and f-MWCNTs/GCE were also fabricated.

### Real sample preparation

The human blood serum sample was collected from the health centre, BHU, Varanasi for the preparation of a real sample. The collected blood serum sample was diluted 100 times in 0.1 M PBS (pH 7.0) to prevent any interference

**Fig. 1** Schematic illustration for the preparation of Co-Nd/Al<sub>2</sub>O<sub>3</sub>@fMWCNTs nanocomposite



present in the sample. The electrochemical measurements were performed by taking a sample in an electrochemical cell, and then spiking it with a pre-defined amount of EP. The analysis was based on the standard addition method. Similarly, human urine was collected and electrochemical analysis was done as prescribed earlier.

## Results and discussion

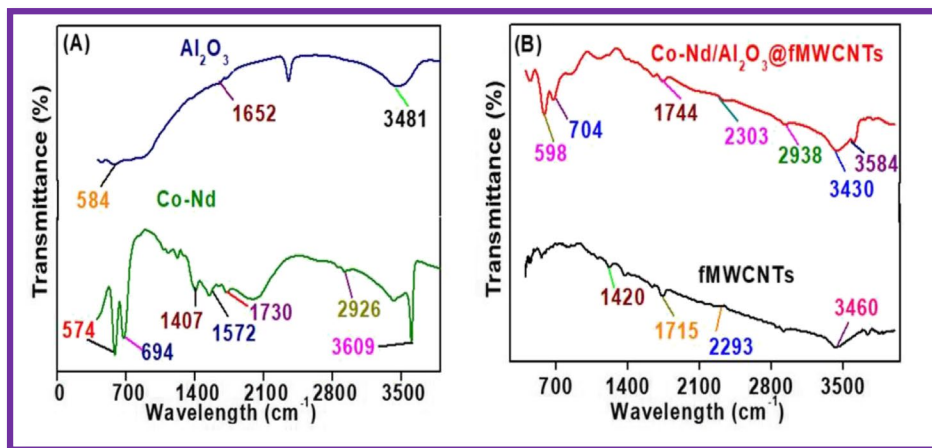
### Physical characterizations

#### FT-IR studies

Figure 2A and B show the FT-IR spectra of Co-Nd bimetallic nanoparticles, Al<sub>2</sub>O<sub>3</sub> nanoparticles, fMWCNTs and

Co-Nd/Al<sub>2</sub>O<sub>3</sub>@fMWCNTs nanocomposite. In the FT-IR spectra of Co-Nd bimetallic nanoparticles as shown in Fig. 2A (green solid curve), the peaks at 574 cm<sup>-1</sup> and 694 cm<sup>-1</sup> are due to the stretching vibration of the Co–O and Nd–O bonds, respectively. In the case of Co<sub>2</sub>O<sub>3</sub>, the additional peak at 1572 cm<sup>-1</sup> is due to the asymmetric vibration of the carboxylate ion (Kudlash et al. 2008). Moreover, the peak at 2926 cm<sup>-1</sup> and 3609 cm<sup>-1</sup> is due to asymmetric vibration of the methylene group and O–H stretching vibration, respectively, in Nd<sub>2</sub>O<sub>3</sub> (Ahmadi et al. 2020). In the FT-IR spectra of Al<sub>2</sub>O<sub>3</sub> nanoparticles as represented in Fig. 2A (blue solid curve), a wide band in the range of 550–1100 cm<sup>-1</sup> was observed, which is associated with Al–O stretching vibrations. Moreover, a large absorption band at 3481 cm<sup>-1</sup> was owing to O–H stretching vibration (Latha et al. 2017). The IR spectra of fMWCNTs are

**Fig. 2** FT-IR spectra. **A** Co-Nd bimetallic nanoparticles (green solid curve) and alumina nanoparticles (blue solid curve). **B** Functionalized MWCNTs (black solid curve) and Co-Nd/Al<sub>2</sub>O<sub>3</sub>@fMWCNTs nanocomposite (red solid curve)



described in Fig. 2B (black solid curve), where the peaks at  $1420\text{ cm}^{-1}$  and  $1715\text{ cm}^{-1}$  correspond to the aromatic C=C stretching vibration and the stretching vibration of C=O from -COOH group, respectively. Furthermore, the peaks at  $2293\text{ cm}^{-1}$  and  $3460\text{ cm}^{-1}$  are related to CH and OH stretching vibrations, respectively (Gupta and Saleh 2011). The IR spectra of the Co-Nd/Al<sub>2</sub>O<sub>3</sub>@fMWCNTs nanocomposite as mentioned in Fig. 2B (red solid curve) show peaks at  $3430$  and  $3584\text{ cm}^{-1}$  due to the O-H stretching vibration of Al<sub>2</sub>O<sub>3</sub> and fMWCNTs, respectively. Furthermore, peaks at  $2938$  and  $2303\text{ cm}^{-1}$  are due to asymmetric vibration of methylene group and CH stretching in Nd<sub>2</sub>O<sub>3</sub> and fMWCNTs, respectively. Moreover, peak at  $1744\text{ cm}^{-1}$  is due to aromatic C=C stretching vibration in fMWCNTs. The Co-O and Nd-O bands in Co-Nd/Al<sub>2</sub>O<sub>3</sub>@fMWCNTs nanocomposite appear at  $598$  and  $704\text{ cm}^{-1}$  respectively (Kudlash et al. 2008; Ahmadi et al. 2020). The appearance of these distinct peaks proved that the Co-Nd/Al<sub>2</sub>O<sub>3</sub>@fMWCNTs nanocomposite had been successfully prepared.

### XRD spectra

XRD spectra are used to determine the crystalline nature of the synthesised nanomaterials. The peaks at  $2\theta$  value of  $14.17^\circ$  (101),  $28.12^\circ$  (110),  $30.40^\circ$  (400),  $39.92^\circ$  (311),  $42.97^\circ$  (222) and  $54.33^\circ$  (511) are due to Co (JCPDS no. 9–418) and Nd (JCPDS no. 21–0579) nanoparticles that affirm the presence of Co-Nd nanoparticles as shown in XRD spectra of Co-Nd bimetallic nanoparticles (Fig. 3A) (Raza et al. 2016; Chen et al. 2017; Ahmadi et al. 2020). Furthermore, using the Debye–Scherer ( $D = k\lambda / \beta \cos \theta$ ) (Bhoi et al. 2020), its crystalline size was determined to be  $2.08\text{ nm}$ , where  $D$ ,  $k$ ,  $\lambda$ ,  $\beta$  and  $\theta$  signify average crystalline size, constant value, X-rays wavelength, full width at half maxima and angle of diffraction respectively. Figure 3B displays the XRD pattern of alumina nanoparticles where corresponding characteristic peaks at  $25.78^\circ$  (012),  $35.53^\circ$  (122),  $37.15^\circ$  (130),  $45.90^\circ$  (400),  $52.32^\circ$  (204),  $56.81^\circ$  (116) and  $66.04^\circ$  (440) were observed, suggesting the presence of Al<sub>2</sub>O<sub>3</sub> nanoparticles (Yadav et al. 2019). Furthermore, its

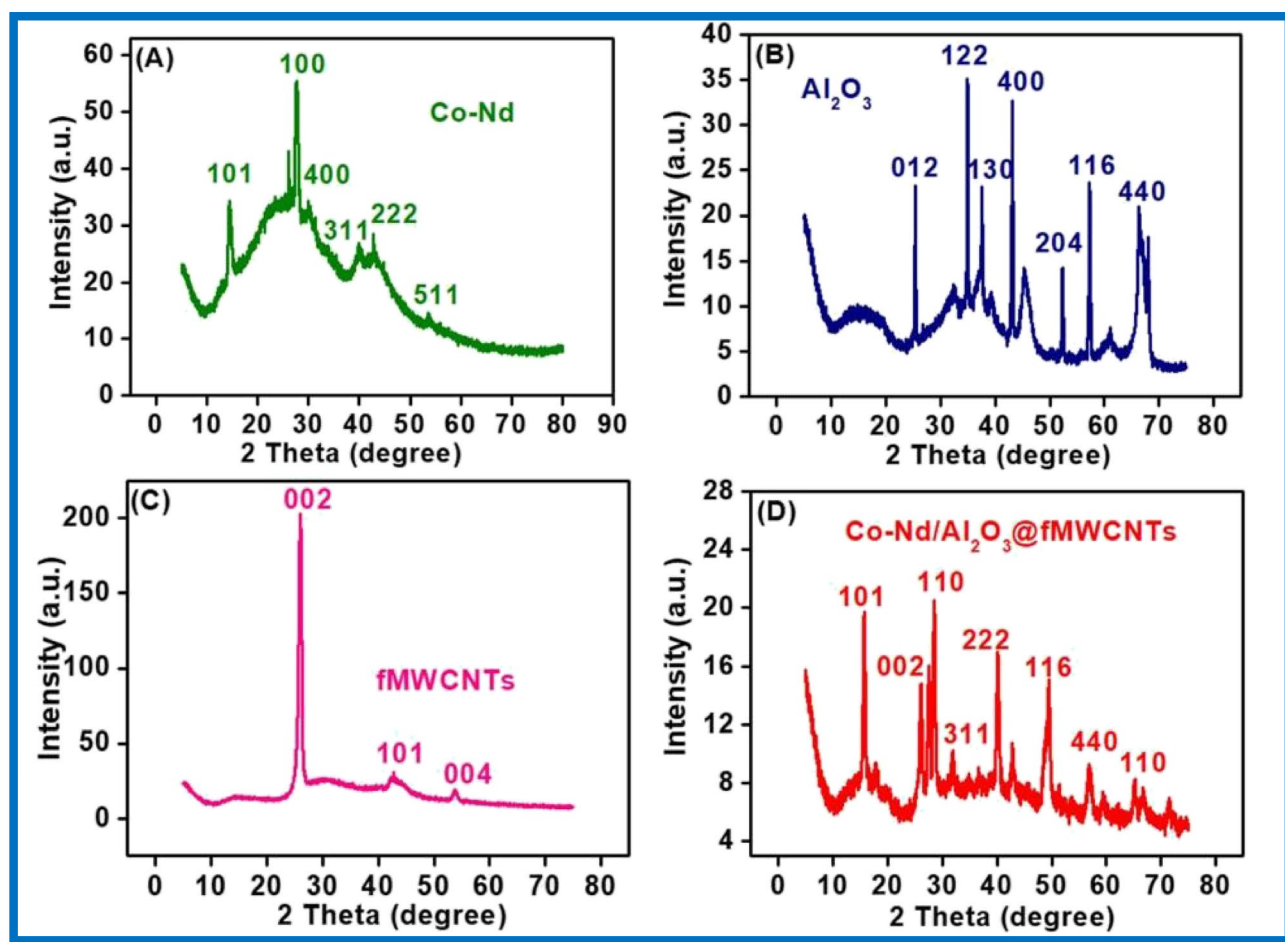


**Fig. 3** XRD spectra of **A** cobalt neodymium bimetallic nanoparticles, **B** alumina nanoparticles, **C** functionalized MWCNTs, and **D** Co-Nd/Al<sub>2</sub>O<sub>3</sub>@fMWCNTs nanocomposite

crystalline size was found to be 72.03 nm. The XRD spectra of fMWCNTs are represented in (Fig. 3C). It displays a peak at  $2\theta$  value of  $25.82^\circ$ ,  $43.67^\circ$ ,  $53.90^\circ$  and  $77.30^\circ$  corresponding to (002), (101), (004) and (110) reflections, respectively (Farbod et al. 2011). Figure 3D demonstrates the XRD pattern of prepared Co-Nd/Al<sub>2</sub>O<sub>3</sub>@fMWCNTs nanocomposite and it shows peak at  $2\theta$  value of  $25.82^\circ$  (002) which is the characteristic peak of fMWCNTs (Farbod et al. 2011). Furthermore, some additional peaks at  $15.56^\circ$  (101),  $28.28^\circ$  (110) and  $39.86^\circ$  (311),  $43.20^\circ$  (222) confirm the existence of Nd (Chen et al. 2017) (Ahmadi et al. 2020) and Co nanoparticles (Raza et al. 2016) in the prepared nanocomposite. Moreover, peaks at  $57.42^\circ$  (116),  $65.29^\circ$  (440) and  $77.92^\circ$  (110) indicate the presence of Al<sub>2</sub>O<sub>3</sub> and fMWCNTs in the fabricated Co-Nd/Al<sub>2</sub>O<sub>3</sub>@fMWCNTs nanocomposite material (Yadav et al. 2019). As a result, of the effective synthesis of the Co-Nd/Al<sub>2</sub>O<sub>3</sub>@fMWCNTs nanocomposite, the XRD data supports the existence of Co-Nd bimetallic nanoparticles, Al<sub>2</sub>O<sub>3</sub> nanoparticles and fMWCNTs.

### UV-visible studies

The dispersions of Al<sub>2</sub>O<sub>3</sub> nanoparticles, Co-Nd nanoparticles, functionalized MWCNTs and Co-Nd/Al<sub>2</sub>O<sub>3</sub>@fMWCNTs nanocomposite were prepared in ethanol for UV-visible spectroscopy. The UV-visible spectra of Co-Nd bimetallic nanoparticles are shown in Fig. 4a, with absorption bands at 295 and 435 nm, respectively, which could be attributed to charge transfer from O<sup>2-</sup> to Co<sup>3+</sup> (Bala et al. 2004) and O-Nd (Prabu et al. 2018) respectively. Figure 4b depicts the absorption band at 270 nm caused by fMWCNTs (Weng and Neethirajan 2017). Figure 4c depicts a UV-visible study of Al<sub>2</sub>O<sub>3</sub> nanoparticles

with an absorption band at 294 nm, confirming the presence of Al<sub>2</sub>O<sub>3</sub> nanoparticles as previously reported (Al-nassar et al. 2015). Furthermore, a broad peak is seen in the UV-visible spectra of the Co-Nd/Al<sub>2</sub>O<sub>3</sub>@fMWCNTs nanocomposite, as shown in Fig. 4d. The broad band in the range of 230–350 nm could be attributed to the overlapping of the characteristic peaks of alumina, bimetallic nanoparticles and fMWCNTs.

### SEM studies

SEM studies were performed to study the surface morphology of alumina nanoparticles, Co-Nd bimetallic nanoparticles, fMWCNTs and Co-Nd/Al<sub>2</sub>O<sub>3</sub>@fMWCNTs nanocomposite. Figure 5A represents the characteristic SEM image of the prepared alumina nanoparticles. The Co-Nd bimetallic nanoparticle represents a spherical shape with a homogeneous structure (Fig. 5B). Moreover, in the SEM image of functionalized MWCNTs as described in Fig. 5C, the walls of MWCNTs have become curled and damaged due to the exfoliation because of the addition of concentrated HNO<sub>3</sub> on the pristine MWCNTs. The Co-Nd bimetallic nanoparticles are homogeneously dispersed over the cylindrical surface of fMWCNT as shown in Fig. 5D. Furthermore, because of the enormous surface area offered by fMWCNTs, alumina and Co-Nd bimetallic nanoparticles are tightly bound to the fMWCNTs walls, boosting conductivity. When coated on GCE, the well distributed alumina and Co-Nd bimetallic nanoparticles on fMWCNTs provide a large surface area, which may result in improved conductivity. The existence of elements such as C, O, Co, Al and Nd in the nanocomposite was verified by EDAX analysis as shown in Fig. 5E.

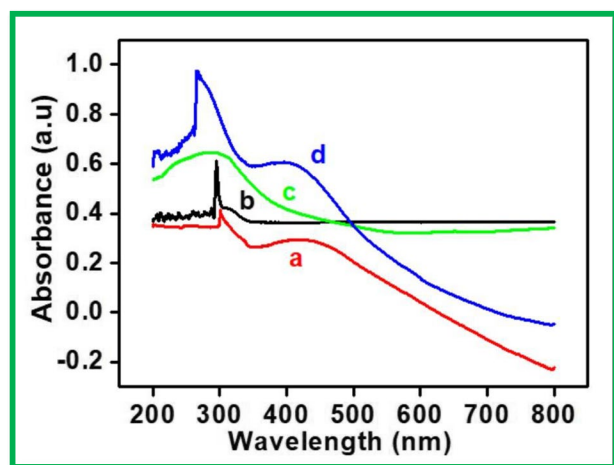


**Fig. 4** UV-visible spectra of **a** alumina nanoparticles, **b** cobalt neodymium bimetallic nanoparticles, **c** functionalized MWCNTs, and **d** Co-Nd/Al<sub>2</sub>O<sub>3</sub>@fMWCNTs nanocomposite

### TEM studies

TEM and selected area electron diffraction (SAED) were used to examine the nanomaterial structure and crystal pattern, respectively. The TEM images under different magnifications of the prepared Co-Nd/Al<sub>2</sub>O<sub>3</sub>@fMWCNTs nanocomposite are described in Fig. 6A and B. From these figures, it appears that the bimetallic and Al<sub>2</sub>O<sub>3</sub> nanoparticles are spherical in shape, but some of them are also present in cluster form and these nanoparticles are attached to the tubular walls of the fMWCNT surface. Figure 6C illustrates the high-resolution TEM image of the prepared Co-Nd/Al<sub>2</sub>O<sub>3</sub>@fMWCNTs where lattice spacing was observed to be 0.325 nm. The SAED pattern consists of bright spots and rings, indicating the crystalline nature of the prepared Co-Nd/Al<sub>2</sub>O<sub>3</sub>@fMWCNTs nanocomposite. The spots and rings originate from the random orientation of the nanoparticles around fMWCNTs as represented in Fig. 6D.

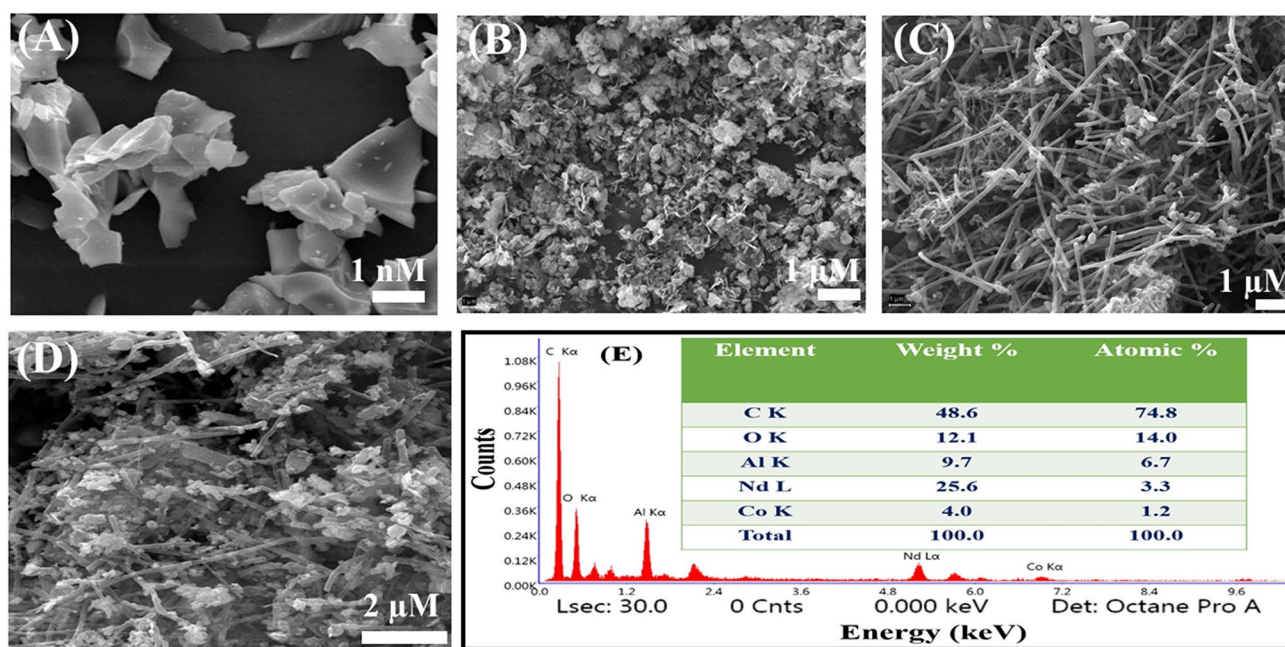


**Fig. 5** SEM image of **A** alumina nanoparticles, **B** cobalt neodymium bimetallic nanoparticles, **C** functionalized MWCNTs, **D** Co-Nd/Al<sub>2</sub>O<sub>3</sub>@fMWCNTs nanocomposite, and **E** EDAX report of Co-Nd/Al<sub>2</sub>O<sub>3</sub>@fMWCNTs nanocomposite

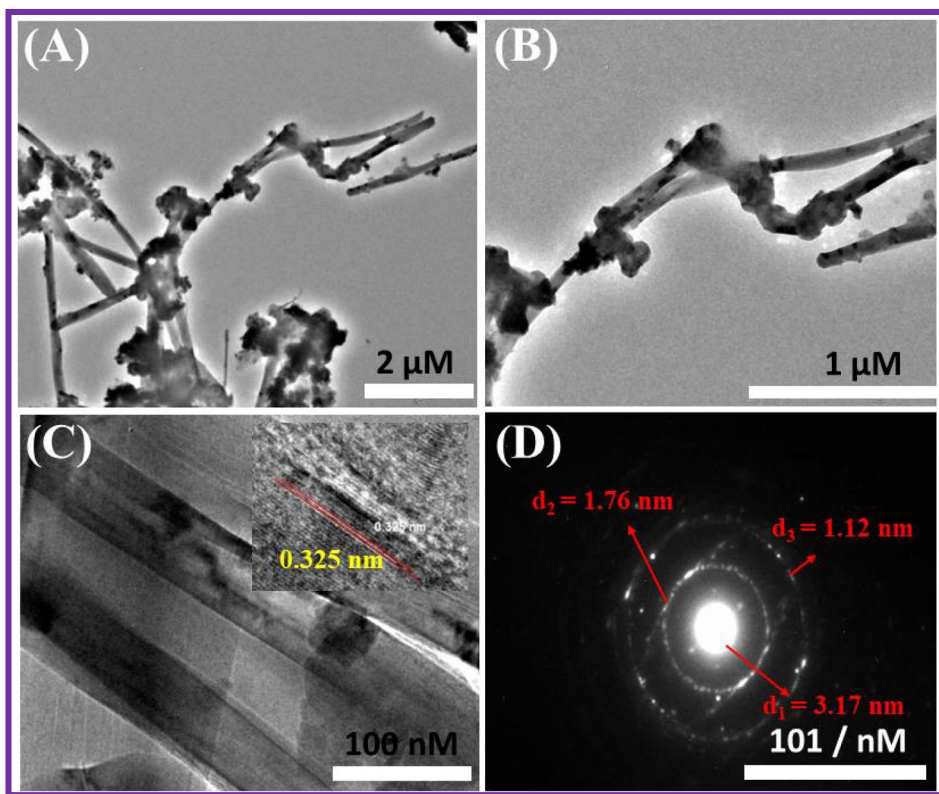
### Electrochemical characterisation of the prepared electrode

EIS studies are used to analyse the electrochemical characteristics of the synthesised nanocomposite materials, since it is a potent technique for examining the electrochemical charge transfer processes at the electrode–electrolyte surface. As shown in Fig. 7A, the Nyquist plot of various modified GCE in the 0.1 Hz to 10 kHz frequency range towards 5 mM [Fe(CN)<sub>6</sub>]<sup>3−/4−</sup> in KCl (0.1 M) is divided into two parts: semicircular and linear components, which represent electron transfer and diffusion-limited processes, respectively. The diameter describes the electron transfer resistance ( $R_{ct}$ ), which regulates the electron transfer kinetics involved, and the semicircular component is noticed at high frequency ranges. A modified Randles equivalent circuit model (*c.f.* Figure 7B) was used to fit the impedimetric spectrum of the modified Co-Nd@Al<sub>2</sub>O<sub>3</sub>-fMWCNTs nanocomposite. Electrolyte resistance ( $R_s$ ), Warburg impedance ( $W$ ), double layer capacitance ( $CPE$ ) and electron transfer resistance are all components of this circuit. The solution's resistance is known as  $R_s$ . The element  $W$  is involved with the diffusion of redox probe ions at the electrode–electrolyte interface. The double layer capacitance is denoted as  $CPE$ . The  $R_{ct}$  values for bare GCE (curve a), Al<sub>2</sub>O<sub>3</sub>/GCE (curve b), Co-Nd/GCE (curve c), fMWCNTs/GCE (curve d) and Co-Nd/Al<sub>2</sub>O<sub>3</sub>@fMWCNTs/GCE (curve e) were found to be 18.2 k $\Omega$ , 13.5 k $\Omega$ , 12.3 k $\Omega$ , 8.49 k $\Omega$  and 904  $\Omega$ , respectively. The  $R_{ct}$  value of Co-Nd/Al<sub>2</sub>O<sub>3</sub>@fMWCNTs/GCE

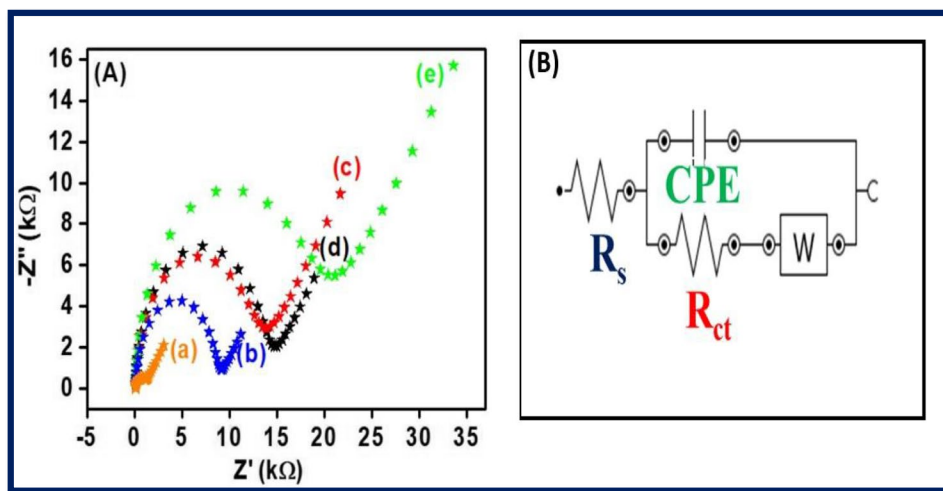
was found to be low in comparison to other modified GCE, signifying that the modified nanocomposite material promotes electron transfer with the addition of electrochemical oxidation.

To compute the heterogeneous rate constant ( $k_{et}$ ) for the 5 mM [Fe(CN)<sub>6</sub>]<sup>3−/4−</sup> redox pair in KCl (0.1 N) at the bare GCE, Al<sub>2</sub>O<sub>3</sub>/GCE, Co-Nd/GCE, fMWCNTs/GCE and Co-Nd/Al<sub>2</sub>O<sub>3</sub>@fMWCNTs/GCE, the equation,  $k_{et} = RT/n^2F^2AR_{ct}C_0$  (Jaiswal and Tiwari 2021), was used where,  $R$  signifies gas constant,  $T$  denotes the temperature in Kelvin while  $n$ ,  $F$ ,  $A$  and  $C_0$  represent the number of electron transfer per redox couple, Faraday constant, geometric surface area of GCE and redox couple concentration in bulk, respectively. The average  $k_{et}$  values for bare GCE, Al<sub>2</sub>O<sub>3</sub>/GCE, Co-Nd/GCE, fMWCNTs/GCE and the prepared Co-Nd/Al<sub>2</sub>O<sub>3</sub>@fMWCNTs/GCE were found to be  $1.03 \times 10^{-5}$  cm<sup>2</sup>/s,  $1.39 \times 10^{-5}$  cm<sup>2</sup>/s,  $1.55 \times 10^{-5}$  cm<sup>2</sup>/s,  $2.20 \times 10^{-5}$  cm<sup>2</sup>/s and  $20.73 \times 10^{-5}$  cm<sup>2</sup>/s, respectively. Co-Nd/Al<sub>2</sub>O<sub>3</sub>@fMWCNTs/GCE has higher values on comparison with other modified GCE, indicating the prepared Co-Nd/Al<sub>2</sub>O<sub>3</sub>@fMWCNTs nanocomposite material resulted in higher electrochemical activity. This might be due to high surface area, large porous structure, and more active centres, and hence, the  $k_{et}$  value for Co-Nd/Al<sub>2</sub>O<sub>3</sub>@fMWCNTs/GCE is found to be maximum. Furthermore, a high  $k_{et}$  value would allow EP to move the electrode–electrolyte interface for electrocatalysis, and it would also support better sensing performance.

**Fig. 6** TEM image of **A** and **B** Co-Nd/Al<sub>2</sub>O<sub>3</sub>@fMWCNTs nanocomposite under various magnifications, **C** HR-TEM image of Co-Nd/Al<sub>2</sub>O<sub>3</sub>@fMWCNTs nanocomposite with lattice spacing, and **D** SAED pattern of Co-Nd/Al<sub>2</sub>O<sub>3</sub>@fMWCNTs nanocomposite with interplanar distance



**Fig. 7** **A** EIS in 5 mM [Fe(CN)<sub>6</sub>]<sup>3-/4-</sup> with 0.1 N KCl at (a) bare GCE, (b) Co-Nd/GCE, (c) Al<sub>2</sub>O<sub>3</sub>/GCE, (d) fMWCNTs/GCE, and (e) Co-Nd/Al<sub>2</sub>O<sub>3</sub>@fMWCNTs/GCE at 20 mV/s. **B** represent equivalent circuit model for fitting EIS response



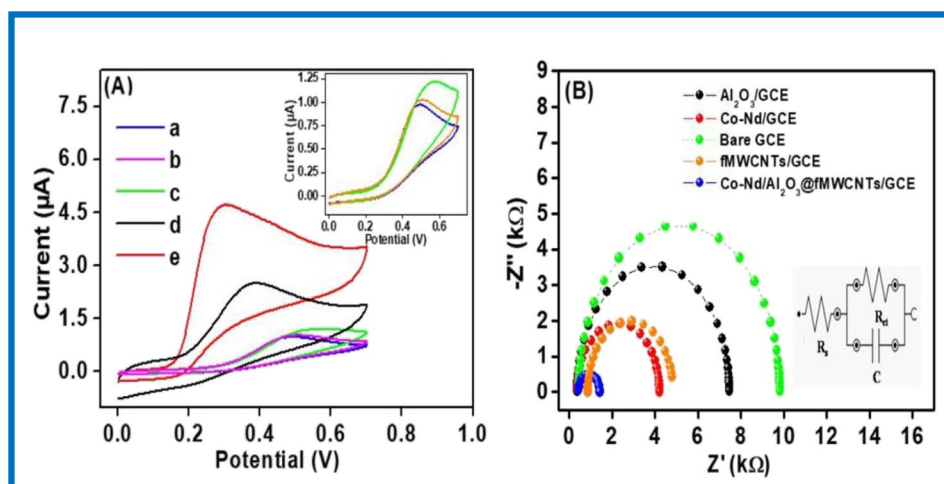
**Electrochemical behaviour of various electrode**

Figure 8A depicts the CV responses of various modified GCE at 20 mV/s in 0.1 M phosphate buffer solution (pH 7.0) by 20 μM EP in the potential range of 0.0 to 0.7. In Fig. 8A, bare/GCE (blue solid curve) and Co-Nd/GCE (orange solid curve) show peaks at 0.48 V and 0.47 V, respectively. Moreover, in the presence of 20 μM, EP oxidation peaks were observed at 0.51 V and 0.36 V is Al<sub>2</sub>O<sub>3</sub>/GCE (green solid

curve) and fMWCNTs/GCE (black solid curve), respectively, with substantially lower current as compared to Co-Nd/Al<sub>2</sub>O<sub>3</sub>@fMWCNTs/GCE. The Co-Nd/Al<sub>2</sub>O<sub>3</sub>@fMWCNTs/GCE (red solid curve) shows a lower oxidation peak potential at 0.28 V and an increased oxidation current in comparison to other modified GCE. It seems interesting to note that fabricated Co-Nd/Al<sub>2</sub>O<sub>3</sub>@fMWCNTs/GCE represents not only an increased anodic peak current but also a reduced peak potential compared to other modified GCE. Furthermore, owing



**Fig. 8** **A** CV of 20  $\mu\text{M}$  EP in 0.1 M phosphate buffer solution (pH 7.0) at (a) bare GCE, (b) Co-Nd/GCE, (c)  $\text{Al}_2\text{O}_3/\text{GCE}$ , (d) fMWCNTs/GCE, and (e) Co-Nd/ $\text{Al}_2\text{O}_3$ @fMWCNTs/GCE at 20 mV/s. **B** EIS data of 20  $\mu\text{M}$  EP in 0.1 M phosphate buffer solution (pH 7.0) at (a) bare GCE, (b) Co-Nd/GCE, (c)  $\text{Al}_2\text{O}_3/\text{GCE}$ , (d) fMWCNTs/GCE, and (e) Co-Nd/ $\text{Al}_2\text{O}_3$ @fMWCNTs/GCE at 20 mV/s. Inset represent equivalent circuit model for fitting EIS response



to the easy modification property of alumina and conductive bimetallic nanoparticles, the conductivity of the fabricated Co-Nd/ $\text{Al}_2\text{O}_3$ @fMWCNTs/GCE was enhanced (Zhang et al. 2018). Moreover, fMWCNTs not only acts as a conductive material but also support nanoparticles, which helps in increasing anodic peak current due to the availability of large active sites (Yang et al. 2015). As a result, due to synergistic effect induced by bimetallic nanoparticle, alumina and fMWCNTs, activation energy barrier gets lowered, which increases oxidation peak current. Therefore, the prepared composite material is better for the detection of EP.

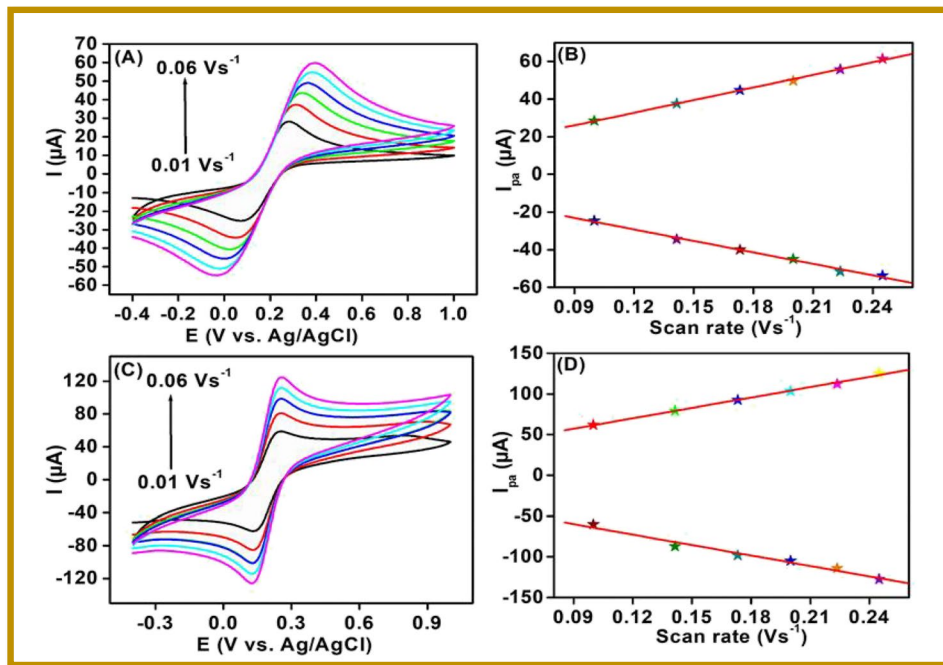
An EIS study was also performed for the investigation of the electrochemical behaviour of EP on various modified GCE. The charge transfer resistance ( $R_{ct}$ ) was measured at the electrode/electrolyte interface through the semicircular diameter of Nyquist plot. Figure 8B displays Nyquist plots of bare GCE (black dashed curve), Co-Nd/GCE (red dashed curve),  $\text{Al}_2\text{O}_3/\text{GCE}$  (green dashed curve) fMWCNTs/GCE (orange dashed curve) and Co-Nd/ $\text{Al}_2\text{O}_3$ @fMWCNTs/GCE (blue dashed curve) which were done in between 0.1 Hz and 10 kHz frequency range in a 0.1 M phosphate buffer solution (pH 7.0). Furthermore, data fitting was done which illustrates  $R_{ct}$  of 9.38 k $\Omega$ , 7.10 k $\Omega$ , 3.84 k $\Omega$ , 3.98 k $\Omega$  and 996  $\Omega$ , on bare GCE,  $\text{Al}_2\text{O}_3/\text{GCE}$ , Co-Nd/GCE, fMWCNTs/GCE and Co-Nd/ $\text{Al}_2\text{O}_3$ @fMWCNTs/GCE respectively. It can be concluded from the above data that Co-Nd/ $\text{Al}_2\text{O}_3$ @fMWCNTs/GCE shows the lowest  $R_{ct}$  value, signifying it to be a better electrical conducting material than all of the other modified GCE. The highest value of  $R_{ct}$  was observed for bare GCE in comparison to other modified GCE. Besides,  $\text{Al}_2\text{O}_3/\text{GCE}$ , Co-Nd/GCE and fMWCNTs/GCE show comparable  $R_{ct}$  which may be due to conducting nature of  $\text{Al}_2\text{O}_3$ , combination of conducting metals and exfoliation in the fMWCNT walls that may be helpful in increasing surface area due to functionalisation respectively. The modified Co-Nd/

$\text{Al}_2\text{O}_3$ @fMWCNTs/GCE displays the least  $R_{ct}$  value due to the synergistic effect of Co-Nd bimetallic, alumina and functionalized MWCNT which helps in enhancing electrical conductivity due to the large effective surface area provided by the developed nanocomposite material. Therefore, the synthesised Co-Nd/ $\text{Al}_2\text{O}_3$ @fMWCNTs nanocomposite material acts as a better electrode modifier because of the easy EP diffusion on the GCE surface that results in showing good electrochemical sensing of the analyte.

### Surface area study

CV was performed to study the electrochemical features of bare GCE Fig. 9A and B and designed Co-Nd/ $\text{Al}_2\text{O}_3$ @fMWCNTs/GCE Fig. 9C and D in 5 mM  $[\text{Fe}(\text{CN})_6]^{3-/4-}$  with 0.1 N KCl as supporting electrolyte at various scan rate (0.01–0.06 V/s). Figure 9B represents  $I_{pa}$  and  $\nu^{1/2}$  plot, which shows the linear variation of anodic peak current with an increase in scan rate and the corresponding linear regression equation for Co-Nd/ $\text{Al}_2\text{O}_3$ @fMWCNTs/GCE are  $I_{pa}$  ( $\mu\text{A}$ ) = 426.19  $\log \nu / \text{Vs}^{-1}$  + 18.9237 ( $R^2 = 0.9983$ ) and  $I_{pc}$  ( $\mu\text{A}$ ) = -428.49  $\log \nu / \text{Vs}^{-1}$  - 21.1729 ( $R^2 = -0.9877$ ). The Randles–Sevcik equation ( $I_{pa} = 2.69 \times 10^5 n^{3/2} A_{eff} D^{1/2} \nu^{1/2} C$ ) was used for calculating the electroactive surface areas of the modified GCE (Maier 2004; Sharma et al. 2012). In this equation,  $I_{pa}$  denotes the anodic peak current (Ampere),  $n$  is the number of electrons ( $n = 2$ ),  $A_{eff}$  is the effective surface area of the electrode ( $\text{cm}^2$ ),  $D$  is the diffusion coefficient ( $7.6 \times 10^{-6} \text{ cm}^2/\text{s}$ ) of  $[\text{Fe}(\text{CN})_6]^{3-/4-}$ ,  $\nu$  is the scan rate (V/s) and  $C$  is the solution concentration ( $\text{mol}/\text{cm}^3$ ). The effective surface area for bare GCE and Co-Nd/ $\text{Al}_2\text{O}_3$ -fMWCNTs/GCE was found to be 0.08 and 0.172  $\text{cm}^2$  respectively. Maximum surface area was established for Co-Nd/ $\text{Al}_2\text{O}_3$ @fMWCNTs/GCE on comparison with other modified GCE, which helps in improving the electrochemical sensing performance of the prepared EP sensor.

**Fig. 9** CV in 5 mM  $[\text{Fe}(\text{CN})_6]^{3-/4-}$  with 0.1 N KCl at various scan rate (0.01–0.06 V/s) of **A** BGCE, **B**  $I_{\text{pa}}$  vs  $(\nu)^{1/2}$ , **C** Co-Nd/Al<sub>2</sub>O<sub>3</sub>@fMWCNTs/GCE, and **D**  $I_{\text{pa}}$  vs  $(\nu)^{1/2}$ .



**Influence of scan rate**

A scan rate study was performed for a better understanding of the mechanism of charge transfer, operating on the Co-Nd/Al<sub>2</sub>O<sub>3</sub>@fMWCNTs/GCE surface. This can be determined by observing the change of anodic peak current and oxidation peak potential as a function of scan rates (Fig. 10A). It displays the CV curves of Co-Nd/Al<sub>2</sub>O<sub>3</sub>@fMWCNTs/GCE at various scan rate (0.01–0.20 V/s) of EP (2 μM) in 0.1 M PBS at pH 7.0. Figure 10B shows that anodic peak current increases linearly with an increase in scan rate. Equation (1) represents the corresponding linear fitted regression equation, and through it, we may conclude that the process occurring on Co-Nd/Al<sub>2</sub>O<sub>3</sub>@fMWCNTs/GCE may be a surface-controlled process (Zhu et al. 2020).

$$I_{\text{pa}} (\mu\text{A}) = 48.835 \log \nu / \text{Vs} - 1 + 0.78102 (R^2 = 0.9918) \tag{1}$$

In addition, to understand the electrochemical oxidation of EP on a fabricated GCE surface, a graph between  $\log I_{\text{pa}}$  vs  $\log \nu$  was plotted (Fig. 10C). Using the slope from the above plot, various processes going on the GCE surface can be inferred. If the slope value is between 0.2 and 0.6, the process would be pure diffusion controlled. If the slope value is between 0.6 and 0.75, the process would be mixed diffusion adsorption controlled and if the slope value is 1.0, the process would be pure adsorption controlled (Jaiswal et al. 2017). The synthesised nanocomposite exhibits a slope of 0.77, which entails an electrochemical process occurring on the GCE surface being purely an adsorption-controlled process. A linear relationship was

observed when a graph (Fig. 10D) between anodic peak potentials ( $E_{\text{pa}}$ ) was plotted, as a function of logarithm of scan rate ( $\log \nu$ ) which implies that irreversible process is occurring on the modified Co-Nd/Al<sub>2</sub>O<sub>3</sub>@fMWCNTs/GCE surface. The corresponding regression Eq. (2) can be written as:

$$E_{\text{pa}} (\text{V}) = 0.0431 \log \nu (\text{V/s}) + 0.28963 (R^2 = 0.9890) \tag{2}$$

Furthermore, the number of electron transfers in the electrochemical oxidation of EP can be calculated using the Tafel plot ( $E_{\text{pa}}$  vs  $\log \nu$ ) and the Laviron Eq. (3), (A 1970; Laviron 1979). According to Laviron equation:

$$E_{\text{pa}} = b \log \nu / 2 + \text{constant} \tag{3}$$

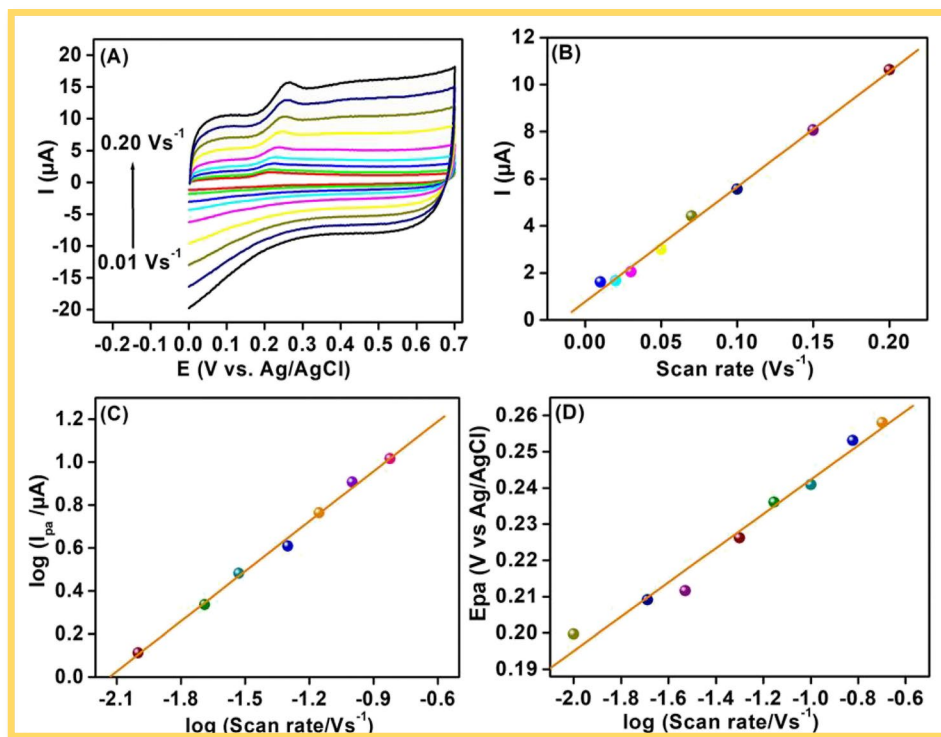
Here,  $E_{\text{pa}}$  is the anodic peak potential,  $\nu$  represents scan rate and  $b$  signifies Tafel slope (A 1970), its value can be known from Eq. (4) which is found to be 0.08996.

$$b = 2.303RT / (1 - \alpha)n F \tag{4}$$

where  $\alpha$  and  $n$  signify charge transfer coefficient and number of electrons transfer, respectively, while  $R$ ,  $F$  and  $T$  are constants with values of  $8.314 \text{ JK}^{-1} \text{ mol}^{-1}$ ,  $96,500 \text{ C mol}^{-1}$ ,  $298 \text{ K}$ , respectively.

Taking  $n$  as 2,  $\alpha$  was calculated as 0.6 for an irreversible process. From this, it can be inferred by using Eq. (7) that on the fabricated GCE surface, an irreversible pure adsorption-controlled process is occurring (Jahanbakhshi 2017). Furthermore, no more additional redox peak potential was observed, indicating it to be an irreversible process.

**Fig. 10** A CV of 2  $\mu\text{M}$  EP in 0.1 M PBS at pH 7.0 at several scan rates (0.01 to 0.02 V/s), **B**  $I$  vs  $(\nu)^{1/2}$ , **C**  $\log I_{pa}$  vs  $\log (\nu)^{1/2}$ , **D**  $E_{pa}$  vs  $\log (\nu)^{1/2}$ .



Furthermore, by using scan rate studies data, the probable mechanism for oxidation of EP can be represented as in Fig. 11. Here, EP undergoes keto-enol tautomerization. The complete electro-oxidation of EP involves two proton and two electron losses and therefore at Co-Nd/Al<sub>2</sub>O<sub>3</sub>@fMWCNTs/GCE electro-oxidation of analyte involves two electron processes as reported earlier (Attia et al. 2017).

### Electrochemical response towards EP

Both CV and DPV were performed to measure linearity, sensitivity and LOD ( $S/N=3$ ) of the modified GCE for EP sensing. In comparison with other electrochemical sensing techniques, differential pulse voltammetry (DPV) provides high selectivity and better sensitivity (El-Sayed et al. 2012). For EP oxidation, CV was done in 0.1 M PBS (pH 7.0) in various concentrations at the Co-Nd/Al<sub>2</sub>O<sub>3</sub>@fMWCNTs/GCE surface. Figure 12A shows a linear increase in response current as EP concentration increase linearly. Using the anodic peak currents (from Fig. 12A) as the analytical response, calibration curves (Fig. 12B) are produced for EP determination. Furthermore, from 0.2 to 14,000  $\mu\text{M}$  EP, current increases linearly with two distinct slopes. Despite two different slopes in the calibration curve, the sensitivity decreases with increasing EP concentrations. The first part of the calibration curve is from 0.2 to 4000  $\mu\text{M}$  with a linear regression equation of  $I_{pa} (\mu\text{A}) = 0.01783 [\text{EP}] (\mu\text{M}) + 0.5913$  ( $R^2 = 0.99615$ ; 0.2 to 4000  $\mu\text{M}$ ) with a LOD of 0.11 with high sensitivity

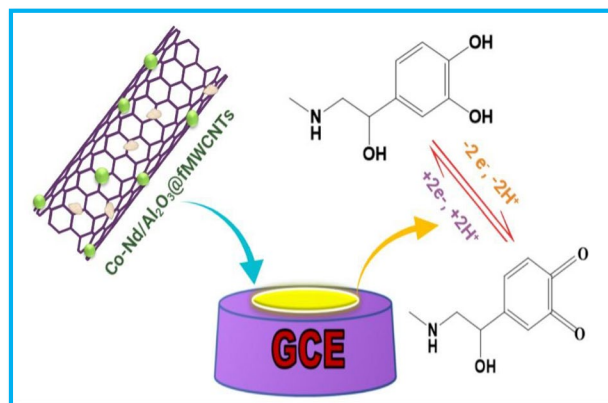
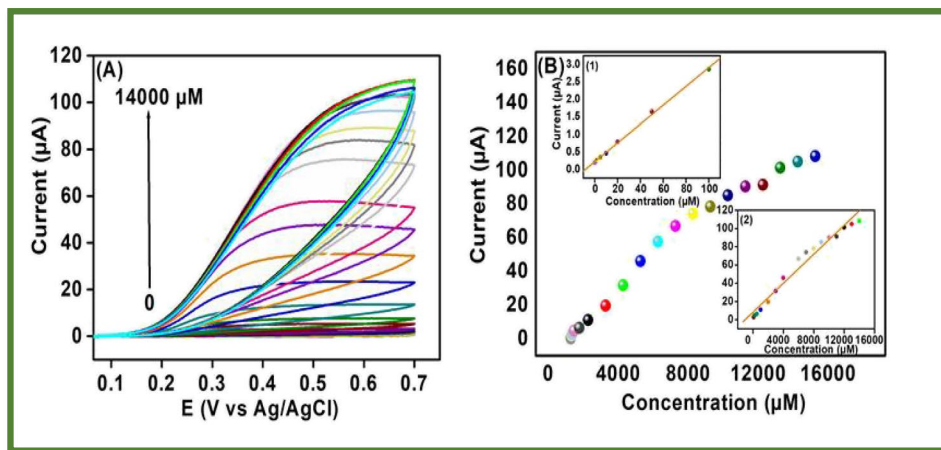


**Fig. 11** Mechanism of EP oxidation on Co-Nd/Al<sub>2</sub>O<sub>3</sub>@fMWCNTs/GCE

of 0.01079  $\mu\text{A}\mu\text{M}^{-1}$  and 4000 to 14,000  $\mu\text{M}$  with a regression equation of  $I_{pa} (\mu\text{A}) = 0.0059[\text{EP}] (\mu\text{M}) + 28.8864$  ( $R^2 = 0.98679$ ; 4000 to 14,000  $\mu\text{M}$ ) with low sensitivity. The limit of detection was 0.11, based on  $3\sigma/m$ , where  $\sigma$  is the standard deviation of the blank and  $m$  is the slope of the calibration plot. Moreover, as EP concentration increases gradually, it provides hindrance for EP diffusion on Co-Nd/Al<sub>2</sub>O<sub>3</sub>@fMWCNTs/GCE surface. Therefore, there might be presence of two different concentration range.

Furthermore, a DPV study was also conducted for the determination of various concentrations of EP at Co-Nd/

**Fig. 12** **A** Electrochemical response of the Co-Nd/Al<sub>2</sub>O<sub>3</sub>@fMWCNTs/GCE nanocomposite towards the sensing of EP by CV in the concentration range of 0.2 to 14,000 μM. **B** Calibration plot, inset 1 for 0.2 to 4000 μM and inset 2 between 4000 and 14,000 μM concentration range



Al<sub>2</sub>O<sub>3</sub>@fMWCNTs/GCE in 0.1 M PBS (pH 7.0). Figure 13A represents the typical DPV response and indicates that EP concentration increases linearly, peak current increases and its corresponding calibration plot is presented in Fig. 13B. Furthermore, the inset of the plot signifies linear relationship between EP concentration and peak current in two different concentration range one from two concentration range one from 0.2 to 4000 μM. Figure 13B (1) with linear regression equation of  $I_{pa} (A) = 0.00323 [EP] (\mu M) + 0.6996$  ( $R^2 = 0.9819$ ; 0.2 to 4000 μM) with LOD of 0.015 and sensitivity of 0.00323  $\mu A \mu M^{-1}$ , and other from 4000 to 14,000 μM with regression equation of  $I_{pa} (A) = 0.0004 [EP] (\mu M) + 0.1108$  ( $R^2 = 0.99205$ ; 4000 to 14,000 μM) and sensitivity of 0.0004  $\mu A \mu M^{-1}$  (Fig. 13B (2)). As shown in Fig. 13B, a dual linear range was observed that might be due to hindrance provided by increased EP concentration for its diffusion on the Co-Nd/Al<sub>2</sub>O<sub>3</sub>@fMWCNTs/GCE surface.

In comparison to CV, DPV provided a lower detection limit for EP sensing. The prepared EP sensor have shown

the advantage of low cost, easy fabrication and a wide concentration range of detection. Moreover, comparison with the earlier reported works as described in Table 1 for EP sensing with the fabricated Co-Nd/Al<sub>2</sub>O<sub>3</sub>@fMWCNTs/GCE was also checked. The prepared Co-Nd/Al<sub>2</sub>O<sub>3</sub>@fMWCNTs/GCE displays wide concentration range (0.2–14,000 μM) in comparison with Au-MWCNT-PANI-TiO<sub>2</sub> (Łuczak 2011), GO/EDDPT/CPE (Tezerjani et al. 2017), NP Au film (Wierzbička and Sulka 2016a) and CoTSPc/MWCNT/GCE (Agboola et al. 2009) respectively. Moreover, NP Au–Ag films (Wierzbička and Sulka 2016b), AuNP/pol(tetramine)/GCE (Taei and Ramazani 2014) and Caffeic acid/GCE (Wang et al. 2006b) exhibit LOD of 5.05 μM, 0.9 μM and 0.6 μM respectively which is higher on comparison with the fabricated Co-Nd@Al<sub>2</sub>O<sub>3</sub>-fMWCNTs/GCE that exhibits very low LOD of 0.015 μM. Therefore, the synthesised Co-Nd/Al<sub>2</sub>O<sub>3</sub>@fMWCNTs/GCE was found to be par/better toward EP oxidation in comparison with previously reported data in terms of wide detection range, better LOD and lower oxidation potential.

**Fig. 13** **A** Electrochemical response of the Co-Nd/Al<sub>2</sub>O<sub>3</sub>@fMWCNTs/GCE nanocomposite towards the sensing of EP by CV in the concentration range of 0.2 to 14,000 μM. **B** Calibration plot, inset 1 for 0.2 to 4000 μM and inset 2 between 4000 and 14,000 μM concentration range

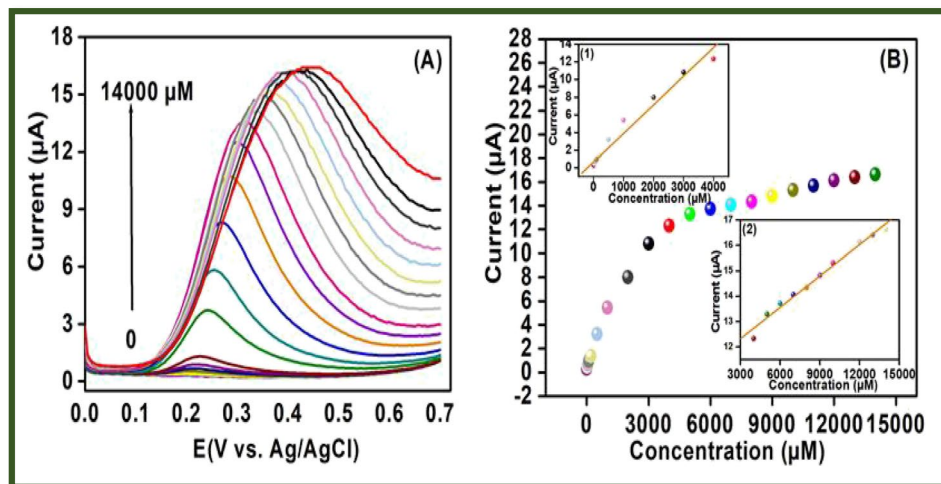


**Table 1** Comparison of the Co-Nd/Al<sub>2</sub>O<sub>3</sub>@fMWCNTs/GCE with other modified electrode for EP sensing

Modified electrode	Techniques	Linear range ( $\mu\text{M}$ )	LOD ( $\mu\text{M}$ )	References
Au-MWCNT-PANI-TiO <sub>2</sub>	DPV	0.077–4.9	0.16	(Łuczak 2011)
GO/EDDPT/CPE	DPV	1.5–600	0.65	(Tezerjani et al. 2017)
NP Au film	DPV	20–190	2.4	(Wierzbička and Sulka 2016a)
CoTSPc/MWCNT/GCE	SWV	0.25–3.5	0.134	(Agboola et al. 2009)
NP Au–Ag films	DPV	10–100	5.05	(Wierzbička and Sulka 2016b)
AuNP/pol(t)risamine/GCE	DPV	3.9–61.8	0.9	(Taei and Ramazani 2014)
Caffeic acid/GCE	CV	2–300	0.6	(Wang et al. 2006b)
Co-Nd/Al <sub>2</sub> O <sub>3</sub> @fMWCNTs/GCE	CV	0.2–14,000	0.11	This work
Co-Nd/Al <sub>2</sub> O <sub>3</sub> @fMWCNTs/GCE	DPV	0.2–14,000	0.015	This work

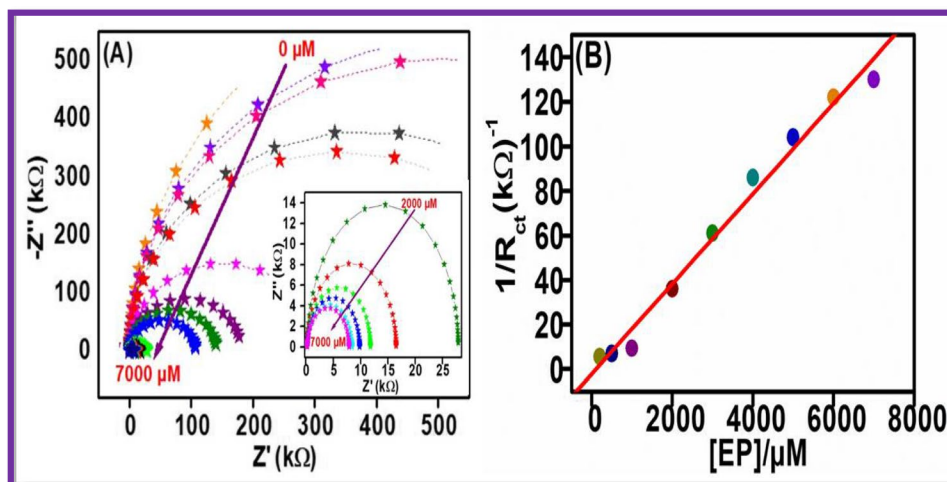
*Au-MWCNT-PANI-TiO<sub>2</sub>*, multiwalled carbon nanotubes and polyaniline nanocomposite doped titanium dioxide on gold electrode; *GO/EDDPT/CPE*, graphene oxide and 2-(5-ethyl-2,4-dihydroxyphenyl)-5,7-dimethyl-4H-pyrido[2,3-d][1,3]thiazine-4-one on carbon paste electrode; *NP Au* film, nanoporous thin gold films; *CoTSPc/MWCNT/GCE*, cobalt (II) tetrasulfophthalocyanine multiwalled carbon nanotubes on glassy carbon electrode; *NP Au–Ag* films, nanoporous spongelike gold-silver electrode; *AuNP/pol(t)risamine/GCE*, gold nanoparticles/poly(2-amino-2-hydroxymethyl-prppane-1,3-diol)modified glassy carbon electrode; *Au/AuNP/DTDPA/CA/AuNPs*, gold electrode modified gold nanoparticles with dithiodipropionic acid and cysteamine; *Caffeic acid/GCE*, poly caffeic acid electrodeposited glassy carbon electrode; *Co-Nd@Al<sub>2</sub>O<sub>3</sub>-fMWCNTs/GCE*, cobalt neodymium nanoparticles doped alumina and functionalized multiwalled carbon nanotubes on glassy carbon electrode; *DPV*, differential pulse voltammetry; *SWV*, square wave voltammetry; *CV*, cyclic voltammetry

## EIS study

The EIS approach was utilised to detect various concentrations of EP at Co-Nd/Al<sub>2</sub>O<sub>3</sub>@fMWCNTs/GCE in 0.1 M PBS ( $pH=7.0$ ) due to its high sensitivity and rapid reaction rate. In the absence of EP, a semi-circle shaped curve is found in the frequency range of 0.1 and 100,000 Hz and when the EP concentration increases, a reduction in the semi-circle diameter can be observed in Fig. 14A. The reason behind this is the eased approach of EP on the prepared Co-Nd/Al<sub>2</sub>O<sub>3</sub>@fMWCNTs/GCE nanocomposite material

that helps in lowering the charge transfer resistance ( $R_{ct}$ ) with increasing concentration. Equivalent electric circuit (as described previously in the inset to (Fig. 8B) was fitted for the interpretation of the EIS data using the Randles and Ershler model, where  $R_{ct}$ ,  $R_s$  and  $C_{dl}$  have their usual meaning as described earlier. With the addition of EP, the parallel combination between  $R_{ct}$  and  $C_{dl}$  results in a depressed semi-circle on the Nyquist impedance plot. To explain the relationship between bulk EP concentration and the  $R_{ct}$  equation ( $R_{ct} = RT/n^2F^2Ak_{ct} [C^0]$ ) was used, where  $R$ ,  $T$ ,  $n$  and  $F$  have usual meaning as already described (Jaiswal

**Fig. 14** **A** EIS data found at Co-Nd/Al<sub>2</sub>O<sub>3</sub>@fMWCNTs/GCE in 0.1 M PBS ( $pH=7.0$ ) having EP in the concentration range from 0 to 7000  $\mu\text{M}$ , inset 1 represents EIS plot of EP concentration ranging from 2000 to 7000  $\mu\text{M}$ . **B** Plot between  $1/R_{ct}$  vs [EP]



et al. 2017). Furthermore,  $A$ ,  $[C_o]$  and  $k_{ct}$  represent geometric surface area of the electrode ( $\text{cm}^2$ ), concentration of redox probe ( $\text{mol}/\text{cm}^3$ ) and charge transfer rate constant dependent on potential. The  $R_{ct}$  at  $[EP] = 0$  was found to be  $1.38 \text{ M}\Omega$ , which is much higher than in the presence of various EP concentrations. The  $R_{ct}$  value shifted from  $1.38 \text{ M}\Omega$  to  $7.64 \text{ K}\Omega$  as EP concentration increased from 0 to  $7000 \mu\text{M}$ . Furthermore, on replacing  $[C_o]$  with  $k_1$  (constant) ( $1/R_{ct} = k_1/[EP]$ ), a linear plot in Fig. 14B (0 to  $7000 \mu\text{M}$ ) was obtained, keeping all other parameters constant, indicating that Co-Nd/ $\text{Al}_2\text{O}_3$ @fMWCNTs/GCE is catalysing EP.

### Chronocoulometry study

Chronocoulometry (Fig. 15A) was used to calculate the surface coverage ( $\Gamma_s$ ) of EP using Anson's equation ( $Q(t) = 2nFAD^{1/2}Ct^{1/2}/\pi^{1/2} + Q_{ads}$ ), where charge, number of electrons transferred ( $n=2$ ), electrode surface area ( $0.07 \text{ cm}^2$ ), diffusion coefficient ( $D = 7.40 \times 10^{-5} \text{ cm}^2/\text{s}$ ), bulk concentration, Faraday constant ( $96,500 \text{ C/mol}$ ) and time are represented by  $Q$ ,  $n$ ,  $A$ ,  $D$ ,  $C$ ,  $F$  and  $t$ , respectively (Wang et al. 2006a). Using the slope of  $Q(t)$  vs.  $t^{1/2}$  plot (Fig. 15B),  $Q_{ads}$  was calculated to be  $1.87 \times 10^{-4} \text{ C}$ . Furthermore,  $\Gamma_s$  can be calculated using the equation,  $\Gamma_s = Q_{ads}/nFA$ , where the terms have similar meaning as described above. This resulted in a surface coverage of  $1.37 \times 10^{-8} \text{ mol cm}^{-2}$  at Co-Nd/ $\text{Al}_2\text{O}_3$ @fMWCNTs/GCE with a  $20 \mu\text{M}$  EP concentration, which is in good agreement with the data reported previously (Agyeman 2017).

### Repeatability, stability and reproducibility of the modified electrode

DPV was used to determine sensor performance by analysing the stability, selectivity and reproducibility of Co-Nd/ $\text{Al}_2\text{O}_3$ @fMWCNTs/GCE-based EP sensors in  $0.1 \text{ M PBS}$

(pH 7.0). The repeatability of the fabricated GCE (Fig. 16A) was determined by measuring the response of a  $2 \mu\text{M}$  EP solution for five successive measurements, yielding a relative standard deviation (RSD) of  $0.09\%$ . In order to ascertain the reproducibility as shown in Fig. 16B, 5 similar Co-Nd/ $\text{Al}_2\text{O}_3$ @fMWCNTs/GCE were made and used for the detection of  $5 \mu\text{M}$  EP solution through DPV. The RSD was found to be  $0.27\%$ , illustrating the good reproducibility of the fabricated Co-Nd/ $\text{Al}_2\text{O}_3$ @fMWCNTs/GCE sensor. Furthermore, stability (Fig. 16C) of the prepared sensor was also examined for 3 weeks through evaluating  $5 \mu\text{M}$  EP solution response at interval of 1 week. The results show that the preliminary DPV value was conserved up to  $92\%$ ,  $90\%$  and  $87\%$ , respectively, at the first, second and third weeks.

### Chemical interference investigation

The limit of tolerance was calculated by taking the highest concentration of interfering analyte, which causes a relative error of nearly  $5\%$  in the EP detection. To examine the selectivity of the EP sensor, interference studies were done as shown in Fig. 16D. It was performed by means of DPV through the addition of some interfering analytes such as  $\text{Na}^+$ ,  $\text{Cl}^-$ ,  $\text{K}^+$ ,  $\text{NO}_3^-$ , glucose, estradiol, para-amino phenol, dopamine, uric acid and ascorbic acid in several folds in  $0.1 \text{ M PBS}$  (pH 7.0) at Co-Nd/ $\text{Al}_2\text{O}_3$ @fMWCNTs/GCE containing a fixed concentration of  $1 \mu\text{M}$  EP. It was found that the fabricated Co-Nd/ $\text{Al}_2\text{O}_3$ @fMWCNTs/GCE shows good selectivity in the presence of several interfering substances with a small change in anodic peak current of epinephrine.

### Real sample analysis

In order to examine the analytical performance of the designed electrochemical EP sensor in real samples such as blood serum and urine, the Co-Nd/ $\text{Al}_2\text{O}_3$ @fMWCNTs composite-modified GCE was tested for EP determination

**Fig. 15** A Chronocoulometric response of 20, 50, 100, 200, 400, 600, and  $800 \mu\text{M}$  on Co-Nd/ $\text{Al}_2\text{O}_3$ @fMWCNTs/GCE. B Plot of  $Q$  vs  $t^{1/2}$

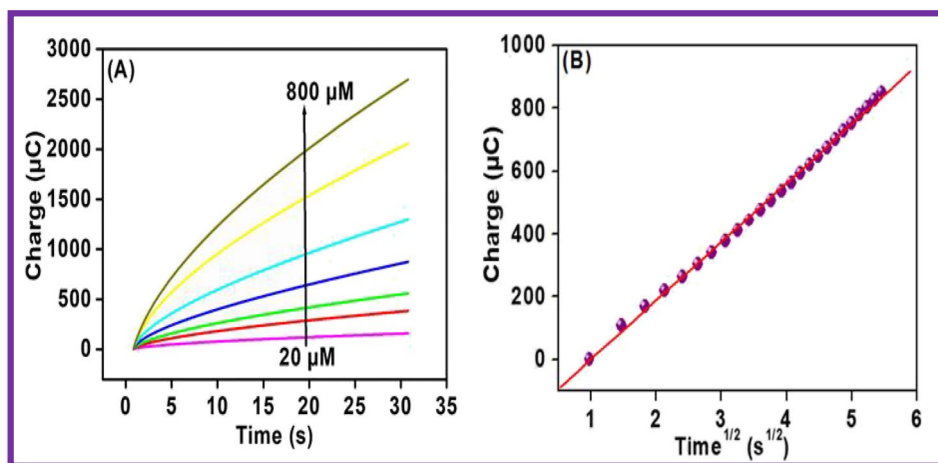


**Fig. 16** **A** Repeatability, **B** reproducibility, **C** stability, and **D** interference studies on Co-Nd/Al<sub>2</sub>O<sub>3</sub>@fMWCNTs/GCE

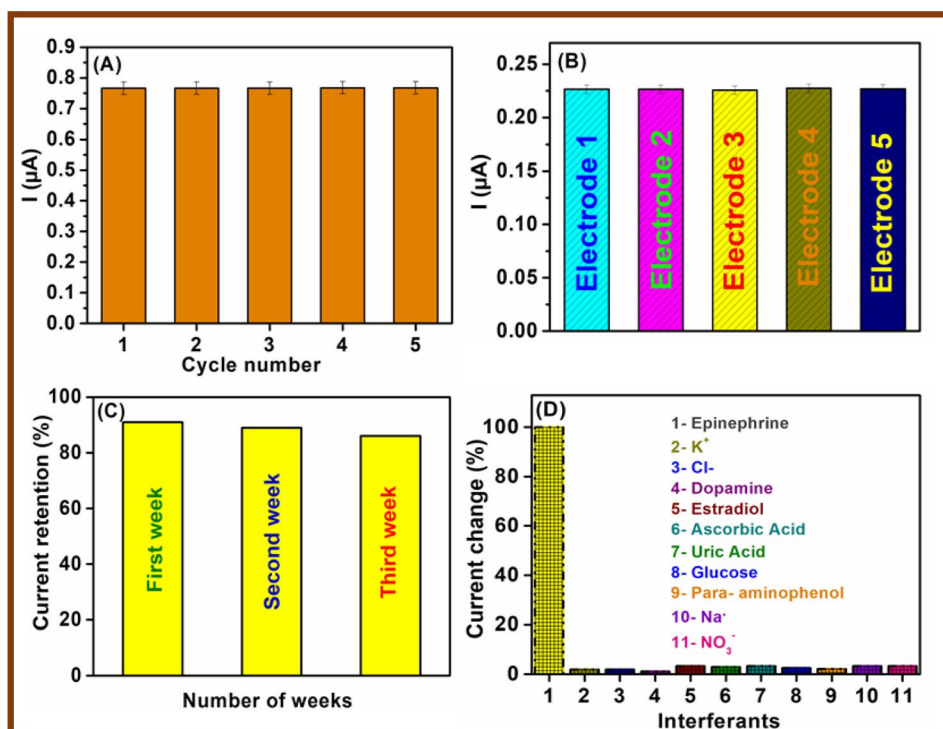


**Table 2** EP determination in blood serum and urine samples

Samples	Added ( $\mu\text{M}$ )	Found ( $\mu\text{M}$ )	Recovery (%)	RSD ( $n=3$ ) (%)
Urine	2	1.96	99.0	0.70
	5	5.10	102.0	1.25
	10	10.37	103.7	2.25
Blood serum	1	1.030	103.0	1.67
	5	4.95	99.0	0.87
	10	9.97	99.7	1.23

using the standard addition method (Table 2). The diluted sample was taken, spiked with a known amount of EP solution, and by using DPV techniques, the electrochemical response was calculated. Moreover, the recovery rate was calculated using the equation (recovery rate (%) = (Found/Added)  $\times$  100). The obtained results are presented in Table 2. In blood serum sample, RSD was found in the range of 0.87 to 1.67%, and the recovery rate was between 99.0 and 103.0%. Furthermore, urine samples displayed an RSD of 0.70 to 2.25% and a recovery rate between 99.0 and 103.7%. Hence, the results obtained were satisfactory. Furthermore, an RSD of less than 5% was obtained for the sensing of EP, indicating that the modified Co-Nd/Al<sub>2</sub>O<sub>3</sub>@fMWCNTs/GCE can be adopted for EP determination in blood serum and urine samples.

## Conclusions

In this experiment, Co-Nd/Al<sub>2</sub>O<sub>3</sub>@fMWCNTs' nanocomposites were successfully synthesised through simple mechanical mixing and then, they were utilised in the modification of GCE. On comparison with other modified GCE, Co-Nd/Al<sub>2</sub>O<sub>3</sub>@fMWCNTs/GCE has shown faster electron transfer and improved catalytic behaviour for the detection of EP that might be due to the synergistic effects of the synthesised Co-Nd bimetallic nanoparticles, alumina nanoparticles and fMWCNTs. According to EIS data, EP had the lowest charge transfer resistance of 996  $\Omega$  at the Co-Nd/Al<sub>2</sub>O<sub>3</sub>@fMWCNTs/GCE surface. In relation to prior investigation, a lower detection limit of 0.015  $\mu\text{M}$  and a wide concentration range of 0.2 to 14,000  $\mu\text{M}$  were found using DPV. Using chronocoulometry, surface coverage ( $\Gamma_s$ ) was calculated to be  $1.37 \times 10^{-8}$  mol  $\text{cm}^{-2}$  at Co-Nd/Al<sub>2</sub>O<sub>3</sub>@fMWCNTs/GCE. The electrochemical sensor based on fabricated Co-Nd/Al<sub>2</sub>O<sub>3</sub>@fMWCNTs/GCE has demonstrated high selectivity and most of the common interferents do not affect in the quantitative EP determination. In addition, the reported Co-Nd/Al<sub>2</sub>O<sub>3</sub>@fMWCNTs/GCE was employed to determine EP in blood serum and urine samples with satisfactory findings, signifying that the as prepared nanocomposite might be highly useful in electrochemical sensing.

**Acknowledgements** SA (Chem./2019-2020/RET-2/Sept-19-term/1/975) and AKS (Chem./2018-19/RET/Sept.18-term/1/4809) are grateful to the University Grants Commission (UGC) in New Delhi for providing research fellowships. RKG thanks UGC for providing DSK-PDF (No. F. 4-2/2006 (BSR)/17-18/0271). The Scheme for Promotion of Academic and Research Collaboration (SPARC-6019), MHRD, India and the IOE incentive grant (Scheme No. 6031) for faculty at BHU are greatly acknowledged for giving financial support. The authors are thankful to Department of Physics for providing the TEM facility. The authors also acknowledge Prof. N. V. Chalapathi Rao, Department of Geology, BHU, for providing SEM and EDAX facilities. The illustrations were created with BioRender.com, and hence the service provider is highly acknowledged.

**Author contribution** SA: methodology, conceptualization, visualisation and writing — original draft; AKS: data curation and formal analysis; RKG: investigation and writing — review and editing; IT: supervision and validation.

**Data availability** Most data generated or analysed during this study are included in this published article.

## Declarations

**Ethics approval** Not applicable.

**Consent to participate** Not applicable.

**Consent to publication** Not applicable.

**Competing interests** The authors declare no competing interests.

## References

- Agboola BO, Vilakazi SL, Ozoemena KI (2009) Electrochemistry at cobalt(II)tetrakisulfophthalocyanine-multi-walled carbon nanotubes modified glassy carbon electrode: a sensing platform for efficient suppression of ascorbic acid in the presence of epinephrine. *J Solid State Electrochem* 13:1367–1379. <https://doi.org/10.1007/s10008-008-0691-3>
- Agyeman AO (2017) Adsorption studies and selective determination of epinephrine at glycerol-clay modified glassy carbon electrode. *Int J Electrochem Sci* 12:9601–9618. <https://doi.org/10.20964/2017.10.56>
- Ahmadi S, Mohammadi L, Rahdar A, et al (2020) Acid dye removal from aqueous solution by using neodymium(III) oxide nanoadsorbents. *Nanomaterials* 10. <https://doi.org/10.3390/nano10030556>
- Al-nassar SI, Mahdi ZF (2015) Study the effect of different liquid media on the synthesis of alumina (Al<sub>2</sub>O<sub>3</sub>) nanoparticle by pulsed laser ablation technique. *Manuf Sci Technol* 3:77–81. <https://doi.org/10.13189/mst.2015.030401>
- Attia A, Rashed N, Fouad M, Wasfy R (2017) Simultaneous Electrochemical determination of articaïne HCl and epinephrine. *Insights Anal Electrochem* 3:1–10. <https://doi.org/10.21767/2470-9867.100018>
- Bala T, Arumugam SK, Pasricha R, et al (2004) Foam-based synthesis of cobalt nanoparticles and their subsequent conversion to CocoreAgshell nanoparticles by a simple transmetallation reaction. *J Mater Chem* 1057–1061. <https://doi.org/10.1039/b315022b>
- Belluzo MS, Ribone MÉ, Lagier CM (2008) Assembling amperometric biosensors for clinical diagnostics. *Sensors* 8:1366–1399. <https://doi.org/10.3390/s8031366>
- Bhoi NK, Singh H, Pratap S (2020) Synthesis and characterization of alumina nanoparticles: a case study. *J Inst Eng Ser C* 101:407–413. <https://doi.org/10.1007/s40032-019-00542-w>
- Burke WJ, Chung HD, Huang JS et al (1988) Evidence for retrograde degeneration of epinephrine neurons in Alzheimer's disease. *Ann Neurol* 24:532–536. <https://doi.org/10.1002/ana.410240409>
- Cañizares P, de Castro MDL (1995) On-line coupling of isolation/in situ concentration integrated with derivative synchronous spectrophotometry for the simultaneous determination of epinephrine and norepinephrine in urine. *Anal Chim Acta* 317:335–341. [https://doi.org/10.1016/0003-2670\(95\)00421-1](https://doi.org/10.1016/0003-2670(95)00421-1)
- Cannon WB, Newton HF, Bright EM et al (1929) Some aspects of the physiology of animals surviving complete exclusion of sympathetic nerve impulses. *Am J Physiol Content* 89:84–107. <https://doi.org/10.1152/ajplegacy.1929.89.1.84>
- Chen KH, Kao MC, Huang SJ, Li JZ (2017) Bipolar switching properties of neodymium oxide RRAM devices using by a low temperature improvement method. *Materials (basel)* 10:1–8. <https://doi.org/10.3390/ma10121415>
- Datsyuk V, Kalyva M, Papagelis K et al (2008) Chemical oxidation of multiwalled carbon nanotubes. *Carbon N Y* 46:833–840. <https://doi.org/10.1016/j.carbon.2008.02.012>
- Eksin E, Bolat G, Kuralay F et al (2015) Preparation of gold nanoparticles/single-walled carbon nanotubes/polyaniline composite-coated electrode developed for DNA detection. *Polym Bull* 72:3135–3146. <https://doi.org/10.1007/s00289-015-1457-6>
- El-Sayed AR, Mohran HS, Abd El-Lateef HM (2012) Corrosion study of zinc, nickel, and zinc-nickel alloys in alkaline solutions by Tafel plot and impedance techniques. *Metall Mater Trans A Phys Metall Mater Sci* 43:619–632. <https://doi.org/10.1007/s11661-011-0908-4>
- Farbod M, Tadavani SK, Kiasat A (2011) Surface oxidation and effect of electric field on dispersion and colloids stability of multiwalled carbon nanotubes. *Colloids Surfaces A Physicochem Eng Asp* 384:685–690. <https://doi.org/10.1016/j.colsurfa.2011.05.041>
- Fernando UPM, Dharmawardhane MP, Subramaniam N et al (2021) Acute respiratory distress syndrome following anaphylactic shock—“A Deadly Duel”—case report and literature review. *Open J Anesthesiol* 11:33–38. <https://doi.org/10.4236/ojanes.2021.112004>
- Garrido EM, Lima JLFC, Delerue-Matos C (1997) Flow injection amperometric determination of L-dopa, epinephrine or dopamine in pharmaceutical preparations. *J Pharm Biomed Anal* 15:845–849. [https://doi.org/10.1016/S0731-7085\(96\)01916-4](https://doi.org/10.1016/S0731-7085(96)01916-4)
- Georgakilas V, Gournis D, Tzitzios V et al (2007) Decorating carbon nanotubes with metal or semiconductor nanoparticles. *J Mater Chem* 17:2679–2694. <https://doi.org/10.1039/b700857k>
- Gupta V, Saleh TA (2011) Syntheses of carbon nanotube-metal oxides composites; adsorption and photo-degradation. *Carbon Nanotub - from Res to Appl*. <https://doi.org/10.5772/18009>
- Hu L, Hecht DS, Grüner G (2010) Carbon nanotube thin films: fabrication, properties, and applications. *Chem Rev* 110:5790–5844. <https://doi.org/10.1021/cr9002962>
- Iost RM, Madurro JM, Brito-Madurro AG et al (2011) Strategies of nano-manipulation for application in electrochemical biosensors. *Int J Electrochem Sci* 6:2965–2997
- Jahanbakhshi M (2017) Mesoporous carbon foam, synthesized via modified Pechini method, in a new dispersant of Salep as a novel substrate for electroanalytical determination of epinephrine in the presence of uric acid. *Mater Sci Eng C* 70:544–551. <https://doi.org/10.1016/j.msec.2016.09.013>
- Jaiswal N, Tiwari I (2021) Self-assembled benzoic acid functionalized graphene oxide sheets with zinc (II) ions: graphene oxide framework; novel material for environmental sensing application. *Synth Met* 276:116754. <https://doi.org/10.1016/j.synthmet.2021.116754>



- Jaiswal N, Tiwari I, Foster CW, Banks CE (2017) Highly sensitive amperometric sensing of nitrite utilizing bulk-modified MnO<sub>2</sub> decorated graphene oxide nanocomposite screen-printed electrodes. *Electrochim Acta* 227:255–266. <https://doi.org/10.1016/j.electacta.2017.01.007>
- Kudlash AN, Vorobyova SA, Lesnikovich AI (2008) Interphase synthesis of colloidal magnetic cobalt nanoparticles. *Magneto-hydrodynamics* 11–18. <https://doi.org/10.22364/mhd.44.1.2>
- Kusuma KB, Manju M, Ravikumar CR et al (2020) Photocatalytic and electrochemical sensor for direct detection of paracetamol comprising  $\gamma$ -aluminium oxide nanoparticles synthesized via sonochemical route. *Sensors Int* 1:100039. <https://doi.org/10.1016/j.sintl.2020.100039>
- Latha P, Prakash K, Karuthapandian S (2017) Enhanced visible light photocatalytic activity of CeO<sub>2</sub>/alumina nanocomposite: synthesized via facile mixing-calcination method for dye degradation. *Adv Powder Technol* 28:2903–2913. <https://doi.org/10.1016/j.apt.2017.08.017>
- Laviron E (1979) General expression of the linear potential sweep voltammogram in the case of diffusionless electrochemical systems. *J Electroanal Chem* 101:19–28. [https://doi.org/10.1016/S0022-0728\(79\)80075-3](https://doi.org/10.1016/S0022-0728(79)80075-3)
- Lin CE, Fang JJ, Deng YJ et al (2004) Capillary electrophoretic studies on the migration behavior of cationic solutes and the influence of interactions of cationic solutes with sodium dodecyl sulfate on the formation of micelles and critical micelle concentration. *J Chromatogr A* 1051:85–94. <https://doi.org/10.1016/j.chroma.2004.08.038>
- Liou TC, Lin SC, Wang HY, Chang WH (2006) Optimal injection volume of epinephrine for endoscopic treatment of peptic ulcer bleeding. *World J Gastroenterol* 12:3108–3113. <https://doi.org/10.3748/wjg.v12.i19.3108>
- Luczak T (2011) Gold electrodes modified with self-assembled layers made of sulphur compounds and gold nanoparticles used for selective electrocatalytic oxidation of catecholamine in the presence of interfering ascorbic and uric acids. *Int J Electrochem* 2011:1–10. <https://doi.org/10.4061/2011/179474>
- Mahnaz D, Ansarian HM (2020) Possible effect of epinephrine in minimizing COVID-19 severity: a review. *J Int Med Res* 48:1–5
- Maier SA (2004) Fundamentals and applications. In: *Plasmonics: fundamentals and applications*. Springer Science+Business Media LLC, pp 1–223. <https://doi.org/10.1007/978-0-387-37825-1>
- Manjunatha JG, Deraman M, Basri NH, Talib IA (2018) Fabrication of poly (Solid Red A) modified carbon nano tube paste electrode and its application for simultaneous determination of epinephrine, uric acid and ascorbic acid. *Arab J Chem* 11:149–158. <https://doi.org/10.1016/j.arabjc.2014.10.009>
- Michałowski J, Hałaburda P (2001) Flow-injection chemiluminescence determination of epinephrine in pharmaceutical preparations using raw apple juice as enzyme source. *Talanta* 55:1165–1171. [https://doi.org/10.1016/S0039-9140\(01\)00536-7](https://doi.org/10.1016/S0039-9140(01)00536-7)
- Ni JA, Ju HX, Chen HY, Leech D (1999) Amperometric determination of epinephrine with an osmium complex and Nafion double-layer membrane modified electrode. *Anal Chim Acta* 378:151–157. [https://doi.org/10.1016/S0003-2670\(98\)00569-8](https://doi.org/10.1016/S0003-2670(98)00569-8)
- Oruch R, Elderbi MA, Khatib HA et al (2014) Lithium: a review of pharmacology, clinical uses, and toxicity. *Eur J Pharmacol* 740:464–473. <https://doi.org/10.1016/j.ejphar.2014.06.042>
- Pérez-López B, Merkoçi A (2012) Carbon nanotubes and graphene in analytical sciences. *Microchim Acta* 179:1–16. <https://doi.org/10.1007/s00604-012-0871-9>
- Prabu RD, Valanarasu S, Geno HAH et al (2018) Effect of neodymium doping on the structural, morphological, optical and electrical properties of copper oxide thin films. *J Mater Sci Mater Electron* 29:10921–10932. <https://doi.org/10.1007/s10854-018-9170-5>
- Raghavendra G, Acharya SK, Pal SK (2014) Preparation of alumina (Al<sub>2</sub>O<sub>3</sub>) nano powder by auto combustion process preparation of alumina (Al<sub>2</sub>O<sub>3</sub>) nano powder by auto combustion process
- Ramgir NS, Yang Y, Zacharias M (2010) Nanowire-based sensors. *Small* 6:1705–1722. <https://doi.org/10.1002/sml.201000972>
- Raymondos K, Panning B, Leuwer M et al (2000) Absorption and hemodynamic effects of airway administration of adrenaline in patients with severe cardiac disease. *Ann Intern Med* 132:800–803. <https://doi.org/10.7326/0003-4819-132-10-20005160-00007>
- Raza MA, Kanwal Z, Riaz S, Naseem S (2016) Synthesis, characterization and antibacterial properties of nano-sized cobalt particles. *Adv Civil Environ Mater Res* 2016:1–7
- Sabbioni C, Saracino MA, Mandrioli R et al (2004) Simultaneous liquid chromatographic analysis of catecholamines and 4-hydroxy-3-methoxyphenylethylene glycol in human plasma: comparison of amperometric and coulometric detection. *J Chromatogr A* 1032:65–71. <https://doi.org/10.1016/j.chroma.2004.01.008>
- Sanghavi BJ, Wolfbeis OS, Hirsch T, Swami NS (2015) Nanomaterial-based electrochemical sensing of neurological drugs and neurotransmitters. *Microchim Acta* 182:1–41. <https://doi.org/10.1007/s00604-014-1308-4>
- Sharma A, Pandey CM, Sumana G et al (2012) Chitosan encapsulated quantum dots platform for leukemia detection. *Biosens Bioelectron* 38:107–113. <https://doi.org/10.1016/j.bios.2012.05.010>
- Spencer JPE, Jenner P, Daniel SE et al (1998) Conjugates of catecholamines with cysteine and GSH in Parkinson's disease: possible mechanisms of formation involving reactive oxygen species. *J Neurochem* 71:2112–2122. <https://doi.org/10.1046/j.1471-4159.1998.71052112.x>
- Struthers AD, Reid JL, Whitesmith R, Rodger JC (2016) Effect of intravenous adrenaline on electrocardiogram, blood pressure, and serum potassium. *Arch Br Hear J* 164:838–843
- Taei M, Ramazani G (2014) Simultaneous determination of norepinephrine, acetaminophen and tyrosine by differential pulse voltammetry using Au-nanoparticles/poly(2-amino-2-hydroxyethyl-propane-1,3-diol) film modified glassy carbon electrode. *Colloids Surfaces B Biointerfaces* 123:23–32. <https://doi.org/10.1016/j.colsurfb.2014.09.005>
- Tezerjani MD, Benvidi A, Dehghani Firouzabadi A et al (2017) Epinephrine electrochemical sensor based on a carbon paste electrode modified with hydroquinone derivative and graphene oxide nano-sheets: simultaneous determination of epinephrine, acetaminophen and dopamine. *Meas J Int Meas Confed* 101:183–189. <https://doi.org/10.1016/j.measurement.2017.01.029>
- Wang L, Bai J, Huang P et al (2006a) Self-assembly of gold nanoparticles for the voltammetric sensing of epinephrine. *Electrochem Commun* 8:1035–1040. <https://doi.org/10.1016/j.elecom.2006.04.012>
- Wang R, Hong QL, Nian BL (2006b) Electrochemical behavior of epinephrine at a glassy carbon electrode modified by electrodeposited films of caffeic acid. *Sensors* 6:80–89
- Weng X, Neethirajan S (2017) Aptamer-based fluorometric determination of norovirus using a paper-based microfluidic device. *Microchim Acta* 184:4545–4552. <https://doi.org/10.1007/s00604-017-2467-x>
- Wierzbicka E, Sulka GD (2016a) Fabrication of highly ordered nanoporous thin Au films and their application for electrochemical determination of epinephrine. *Sensors Actuators, B Chem* 222:270–279. <https://doi.org/10.1016/j.snb.2015.08.066>
- Wierzbicka E, Sulka GD (2016b) Nanoporous spongelike Au-Ag films for electrochemical epinephrine sensing. *J Electroanal Chem* 762:43–50. <https://doi.org/10.1016/j.jelechem.2015.12.013>
- Yadav D, Kumar P, Kapur M, Mondal MK (2019) Phosphate removal from aqueous solutions by nano-alumina for the effective


- remediation of eutrophication. *Environ Prog Sustain Energy* 38:S77–S85. <https://doi.org/10.1002/ep.12920>
- Yang N, Chen X, Ren T et al (2015) Carbon nanotube based biosensors. *Sensors Actuators, B Chem* 207:690–715. <https://doi.org/10.1016/j.snb.2014.10.040>
- Zhang R, Qian J, Ye S et al (2018) Synthesis and enhanced electrochemical activity of Ag-Pt bimetallic nanoparticles decorated MWCNTs/PANI nanocomposites. *J Wuhan Univ Technol Mater Sci Ed* 33:1281–1287. <https://doi.org/10.1007/s11595-018-1964-z>
- Zhu D, Ma H, Zhen Q et al (2020) Hierarchical flower-like zinc oxide nanosheets in-situ growth on three-dimensional ferrocene-functionalized graphene framework for sensitive determination

of epinephrine and its oxidation derivative. *Appl Surf Sci* 526:146721. <https://doi.org/10.1016/j.apsusc.2020.146721>

**Publisher's note** Springer Nature remains neutral with regard to jurisdictional claims in published maps and institutional affiliations.

Springer Nature or its licensor (e.g. a society or other partner) holds exclusive rights to this article under a publishing agreement with the author(s) or other rightsholder(s); author self-archiving of the accepted manuscript version of this article is solely governed by the terms of such publishing agreement and applicable law.

## Authors and Affiliations

Shreanshi Agrahari<sup>1</sup> · Ankit Kumar Singh<sup>1</sup> · Ravindra Kumar Gautam<sup>1</sup> · Ida Tiwari<sup>1</sup> 

✉ Ida Tiwari  
idatiwari@bhu.ac.in

Shreanshi Agrahari  
shreanshiagrahari@gmail.com

Ankit Kumar Singh  
anksingh325@gmail.com

Ravindra Kumar Gautam  
ravindragautam1987@gmail.com

<sup>1</sup> Department of Chemistry (Centre of Advanced Study), Institute of Science, Banaras Hindu University, Varanasi 221005, India